CHAPTER 4

RESULTS AND DISCUSSIONS

4.1 Characterization of PZT sample made by spray dry technique

PZT powders prepared by spray dry technique were calcined at several temperatures and analysed phase formation by x-ray diffractometry to identify the phase change of the samples. The particle sizes of the powder were determined by particle size analyzer. The Scanning Electron Microscopy (SEM) was also used for determining the morphology and particle size.

4.1.1 Thermal Analysis of PZT sprayed powder

The thermograms of DTA and TG indicating the phase transformation and weight loss, respectively, of the spray dried granules at various temperatures are shown in Figure 4.1. The first weight loss accompanied by an endothermic peak is around 100 ^{o}C. This is due to the evaporation of water and volatile residues that generally exist in the powder. The endothermic peak at about 400 ^{o}C may be attributed to the evolution of gases such as NO or NO_2 as indicated by Wang *et al*. [120] and Das *et al.* [121], which can be confirmed by the weight loss in TG curve from about 80 wt% down to 60 wt%. The noticeable exothermic peak at around 530 ^{o}C is possibly due to the crystallization of

PZT phase [122]. This is consistent with the XRD result in Figure 4.2, which shows the growth of PZT cubic phase starting at 500 °C.

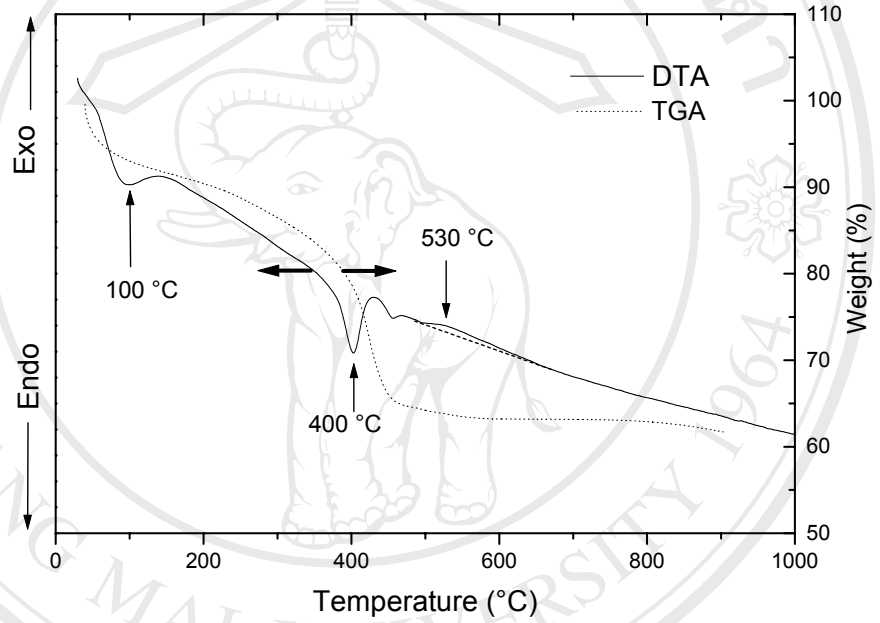

Figure 4.1 DTA and TG thermograms of the spray dried granules.

4.1.2 X-ray Diffraction Results

4.1.2.1 Spray dry powder

The PZT powder calcined at the temperatures of 500 °C, 600 °C, 700 °C, 800 °C and 850 °C was scanned using a Siemens Diffractometer with Ni filtered CuK_α radiation, covering the 2θ ranges of 20°-60°, stepping scan of 0.5° and 1 sec counting time per step was employed. The corresponding diffractograms were compared with JCPDS powder diffraction file of PZT powder [123] as shown in Table 4.1. Figure 4.2 shows X-ray diffractograms of the prepared samples after the calcination, at different calcination temperatures, indicating the phase evolution of the spray dried granules. It can be seen that the PZT phase began to appear at 500 ^oC and became even more pronounced at 850 ^oC. Every peak can be attributed to PZT [123]. No impurities or secondary phases were detected using this XRD method. The formation of the perovskite PZT phase is agreeable to that formed in other methods, such as the coprecipitation method [122] and the mechanochemical method [124].

Table 4.1 JCPDS Powder Diffraction File of PZT powder. [123]

d(Å)	I/I_1	hkl
4.146	9	001
4.036	12	100
2.890	100	101
2.850		110
2.351	15	111
2.073	9	002
2.018	16	200
1.844	5	102
1.810	6	201, 210
1.677	12	112
1.655	25	211
1.446	9	022
1.427	5	220
1.382	2	003
1.361	6	212
1.350		221
1.038	6	103
1.244	2	113
1.220	2	311

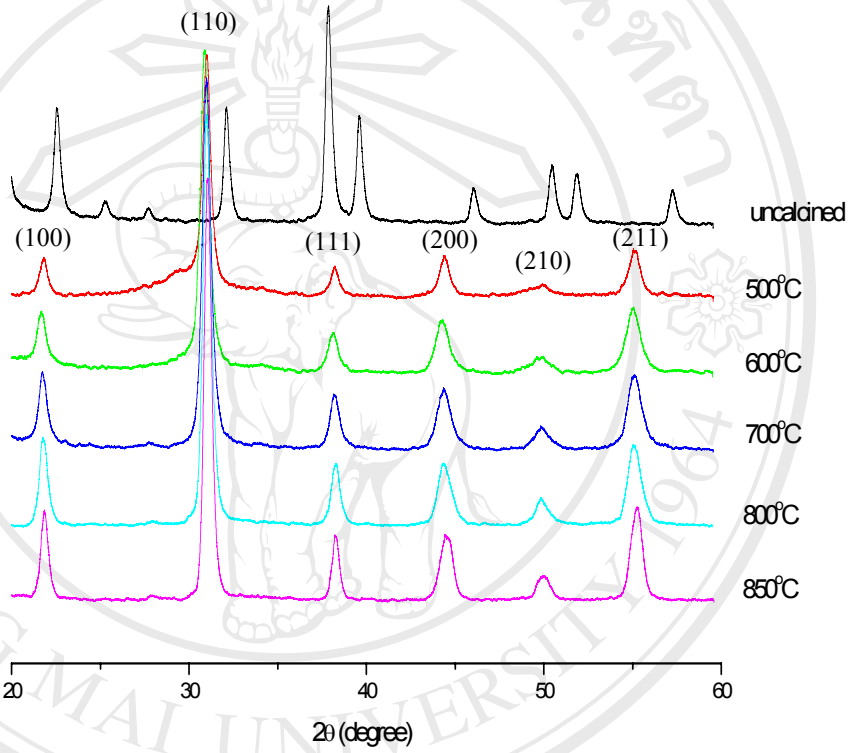

Figure 4.2 XRD patterns of PZT powder made by spray dry technique calcined at different temperature.

4.1.2.2 Spray dry ceramics

The X-ray diffractograms of the PZT ceramics sintered at different sintering temperatures are also shown in Figure 4.3. It can be seen that the impurities were not detected by XRD method. It may be due to the high purity of the samples. Every appeared peaks were corresponding to the PZT phase which matched with the JCPDS file no. 33-784 [123]. However, cubic phase obtained in every sintering conditions.

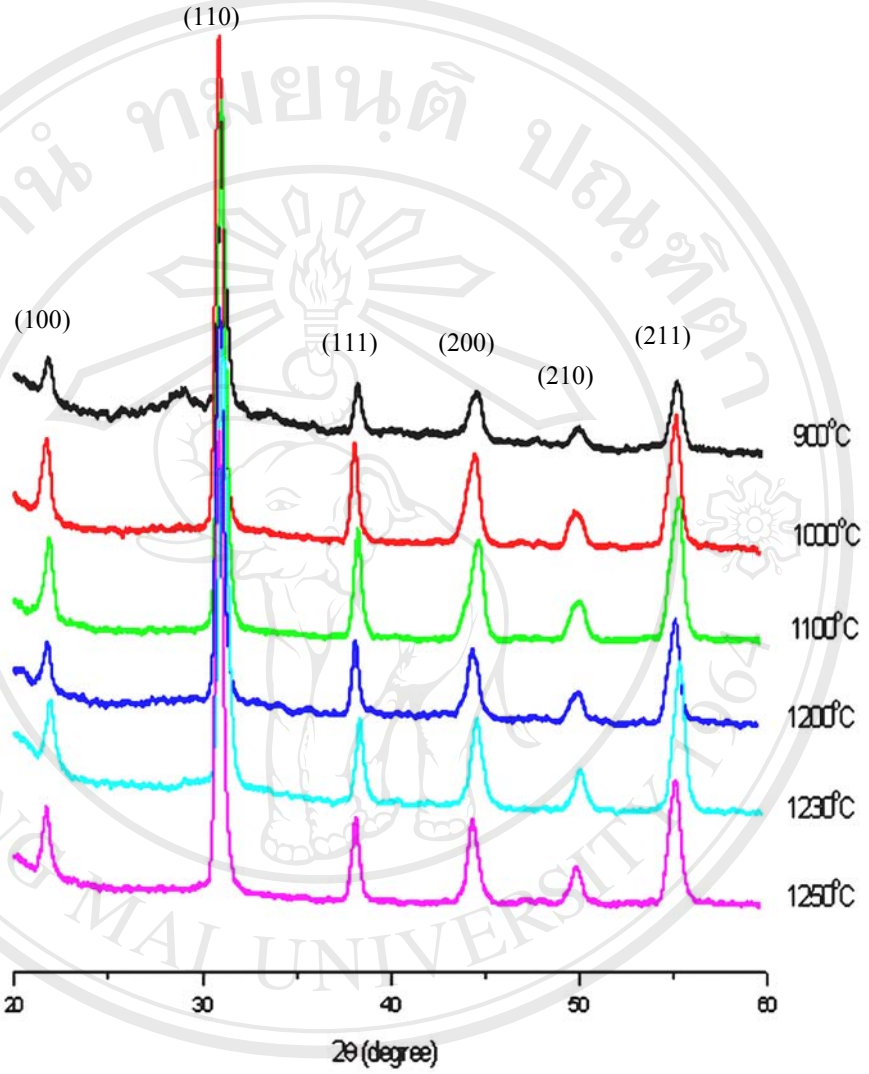

Figure 4.3 XRD patterns of sprayed PZT ceramics sintered with various temperatures.

4.1.3 Determination of the Particle Size

The distribution of particle size is shown in Figure. 4.4-4.6. From the results, it can be seen that the particle size distribution of sprayed powders exhibit the two peaks of particle size average. This could be the effect from the agglomerations of particles. The average particle size is in the range of 1-3 μm. It can be seen that the value of average particle size is increased with the calcining temperature.

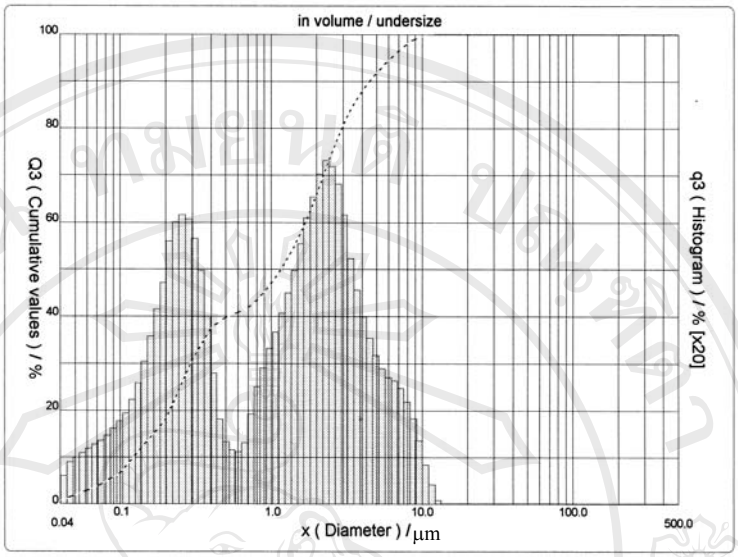

(a)

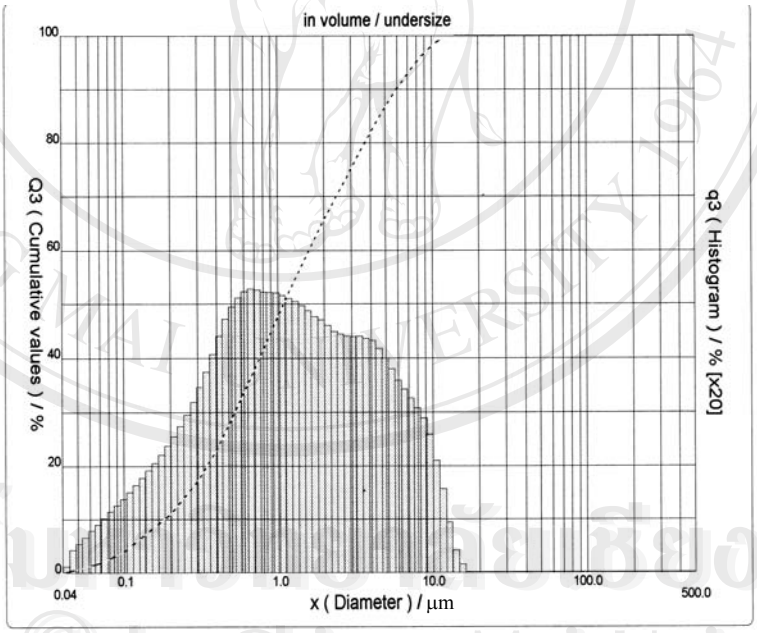

(b)

Figure 4.4 Particle size distribution of PZT sprayed powder calcined at (a) 500 °C and (b) 600 °C

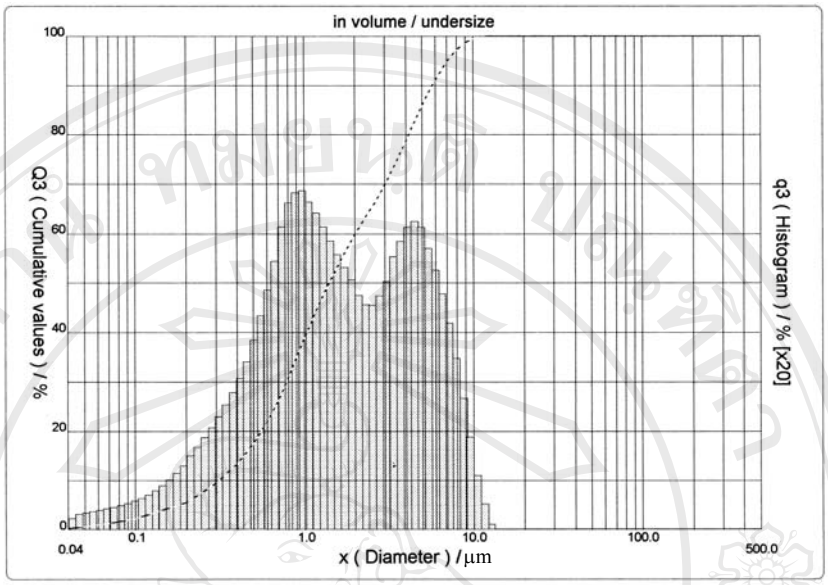

(a)

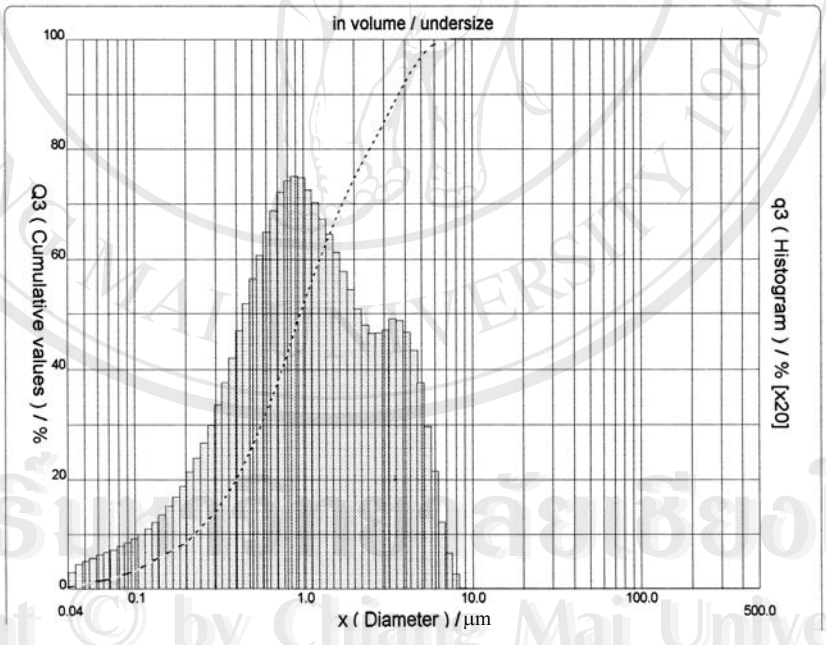

(b)

Figure 4.5 Particle size distribution of PZT sprayed powder calcined at (a) 700 °C and (b) 800 °C

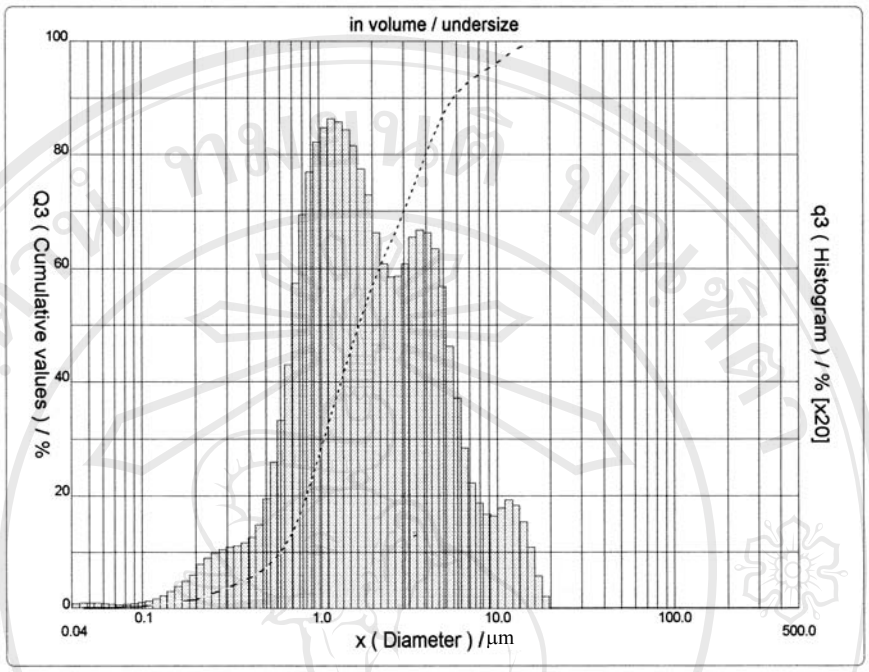

Figure 4.6 Particle size distribution of PZT sprayed powder calcined at 850 °C

4.1.4 Examination of sprayed PZT powder by SEM and TEM

The morphology of the as-sprayed and calcined PZT powders obtained by the spray drying technique are shown in the SEM micrographs (Figure 4.7-4.9). It can be seen that the size of the as-sprayed granules is about 1-2 μm and the shape is almost spherical but with dimples. The granules grew bigger at the higher calcining temperature as generally expected. The same shape was also observed in the spray-dried granules produced by Uematsu *et al*. [125].

In order to confirm the purity of the PZT particles, the EDS and TED analyses were employed. A typical EDS spectrum was illustrated in (Figure 4.11), showing no sign of impurity excepting carbon particles which were sputtered on the sample and a trace amount of Mn dopant. The transmission electron diffraction (TED) patterns of selected area were studied. The typical TED and its corresponding TEM were shown in Figure 4.10. By using the method from Andrews *et al*. [126], the TED spots (Figure. 4.10a) were analysed. It was found that all TED spots are corresponding to the PZT phase [110]. This confirmed the high-purity of the PZT powders. Its corresponding transmission electron micrograph (Figure 4.10b) shows thin layers of PZT locating on top of each other which is contributed to the spots and rings in the TED.

Furthermore, dark field and bright field image of TEM was used for determining the thin layer of PZT ceramic to identify the Mn-dopant phase within bulk of sample (Figure 4.12-4.14). Since the quantity of doping is too low, therefore, the Mn phase cannot be detected by this technique. Dark field image (Figure 4.12) shows the thin

layers of planes. However, the layer is not thin enough to examine the plane by TED. Both of dark and bright fields also indicated the crack line which lie through the sample.

Moreover, the SEM micrographs of as sintered and fracture surface of PZT ceramics sintered at different temperature (900 ^{o}C-1250 ^{o}C) are also shown in Figure 4.15-4.17 and Figure 4.18-4.20, respectively. It can be seen that the normal grain growth and round shape obtained from these samples. Furthermore, the average grain size is in the range of 0.44-2.69 μm for as sintered surface and 0.88-2.60 μm for fracture surface.

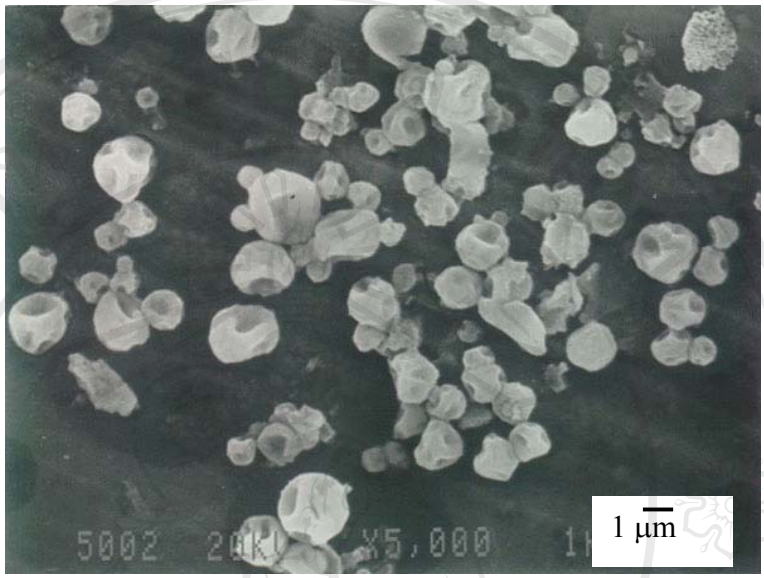

(a)

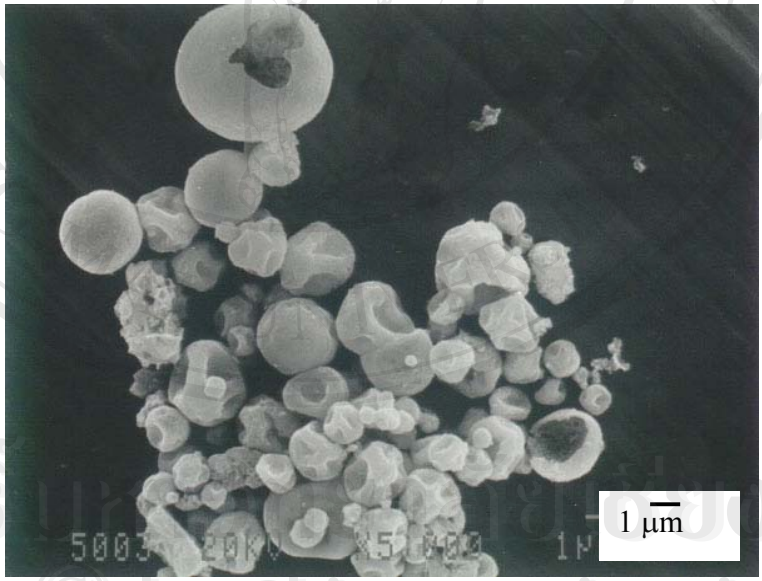

(b)

Figure 4.7 SEM micrographs of sprayed powder (a) uncalcined and (b) calcined at 500 ^{O}C.

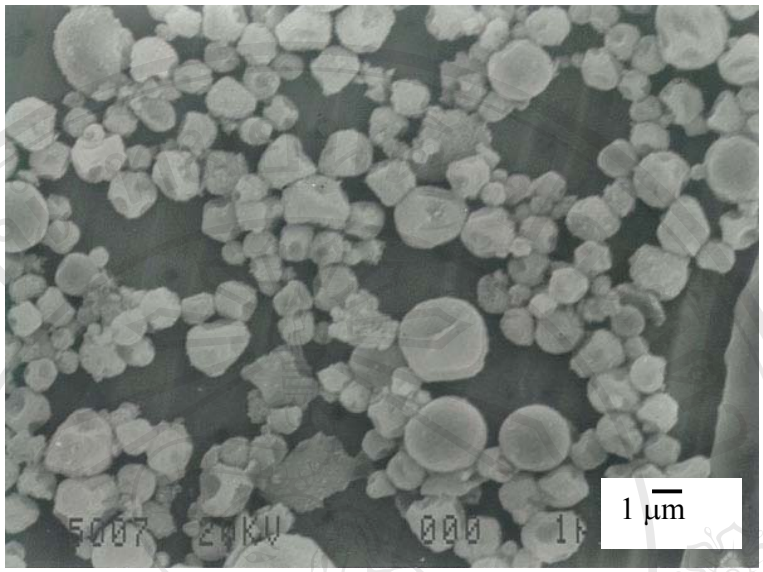

(a)

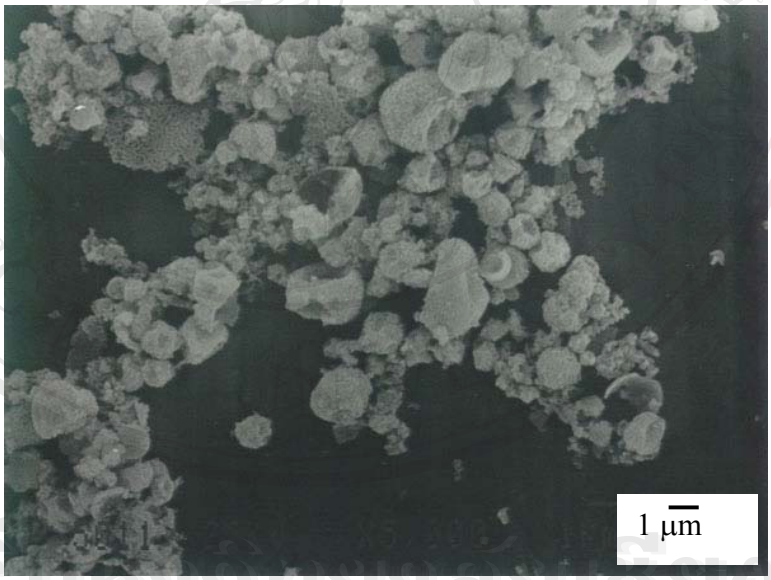

(b)

Figure 4.8 SEM micrographs of sprayed powder calcined at (a) 600 ^{O}C and (b) 700 ^{O}C.

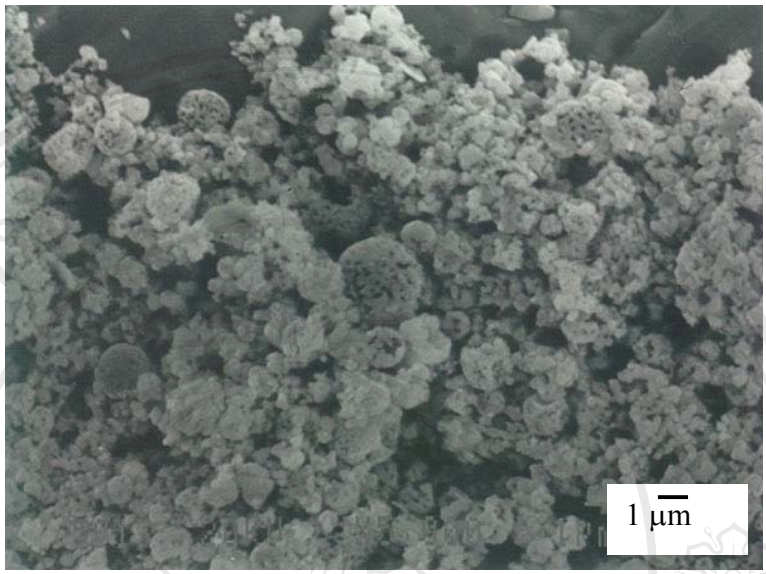

(a)

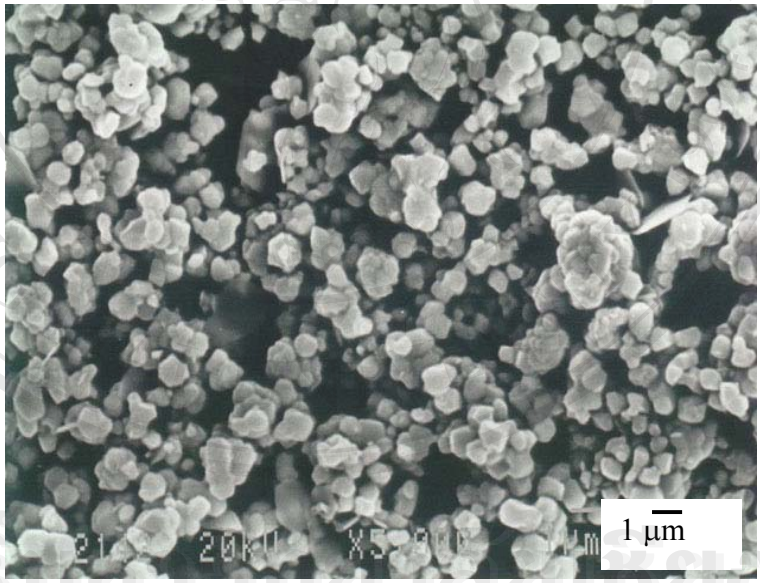

(b)

Figure 4.9 SEM micrographs of sprayed powder calcined at (a) 800 ^{O}C and (b) 850 ^{O}C.

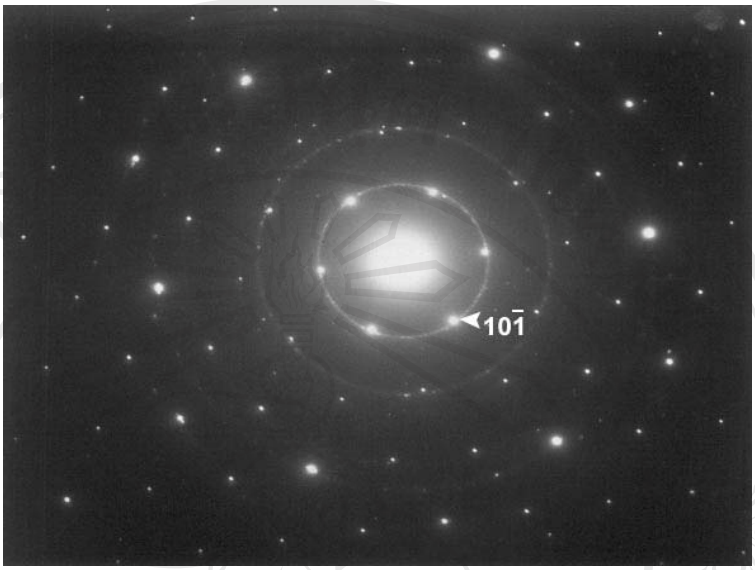

(a)

(b)

Figure. 4.10 TED (a) and TEM (b) micrographs of selected area of PZT powder.

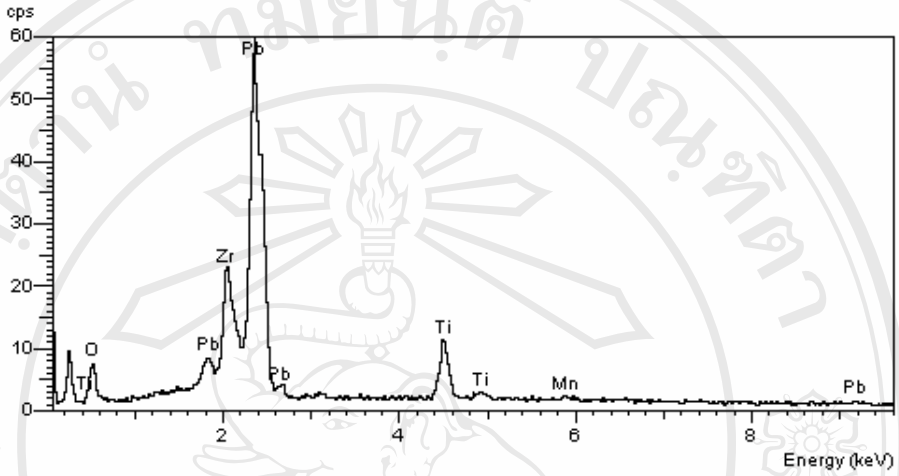

Figure 4.11 EDS spectrum of corresponding PZT powders.

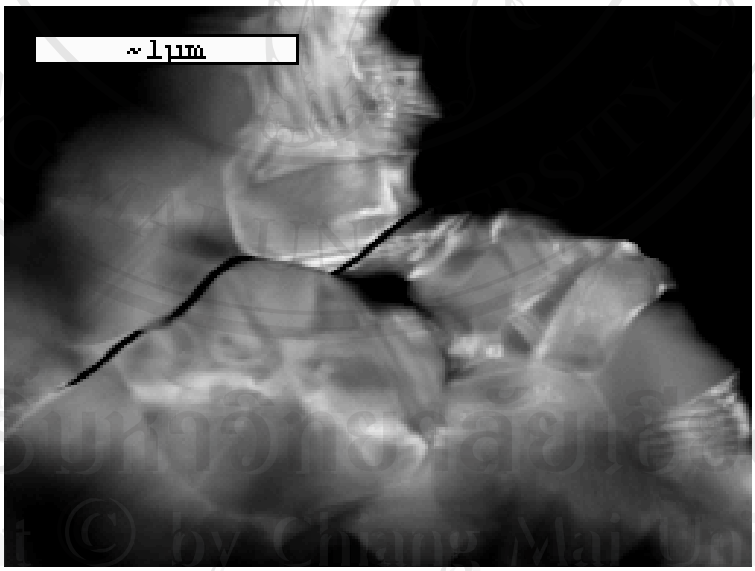

Figure 4.12 The dark field image of PZT ceramics prepared from sprayed powder.

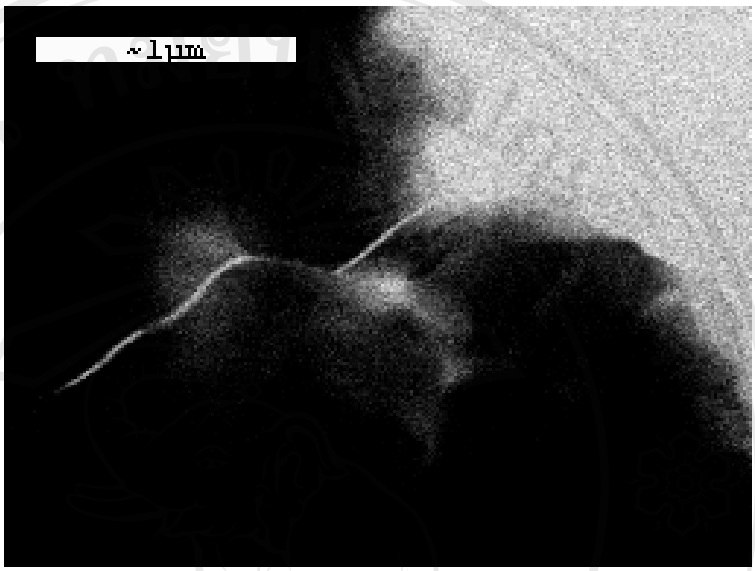

Figure 4.13 The bright field image of PZT ceramics prepared from sprayed powder.

Figure 4.14 The bright field image of PZT ceramics prepared from sprayed powder with different angle.

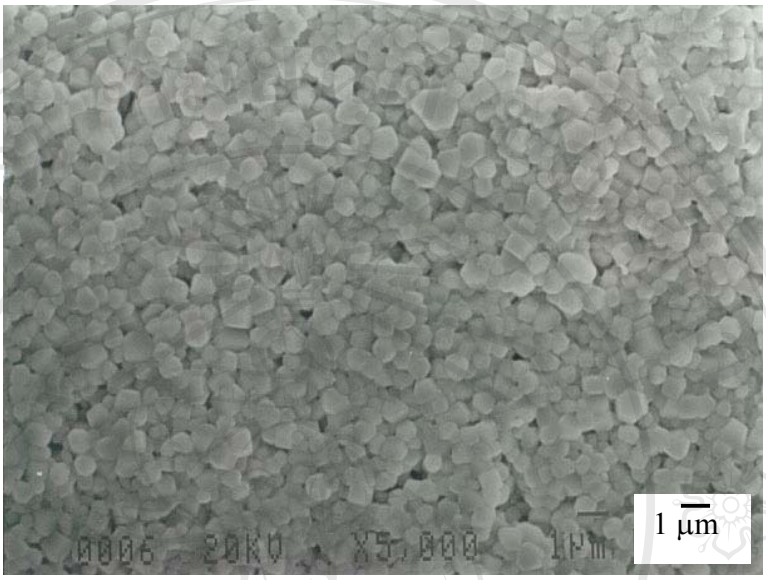

(a)

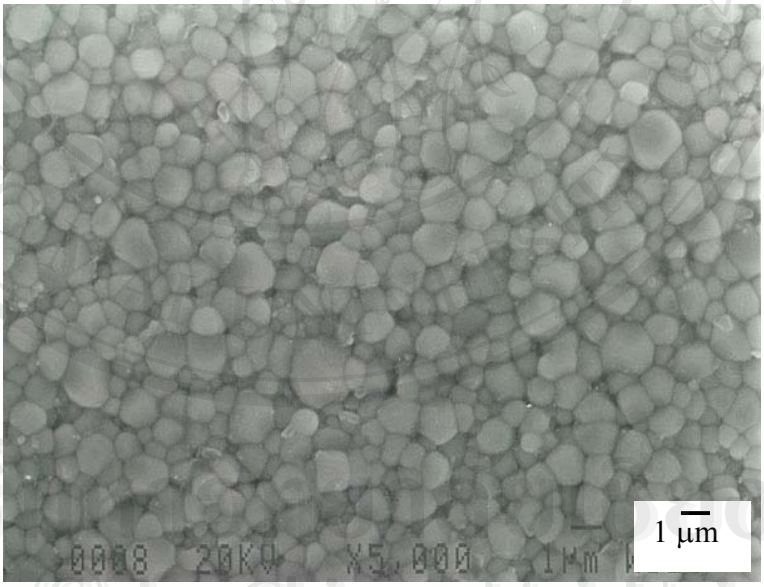

(b)

Figure 4.15 SEM micrographs of as sintered surface of PZT ceramics fabricated from spray dried granules sintered at (a) 900 °C and (b) 1000 °C.

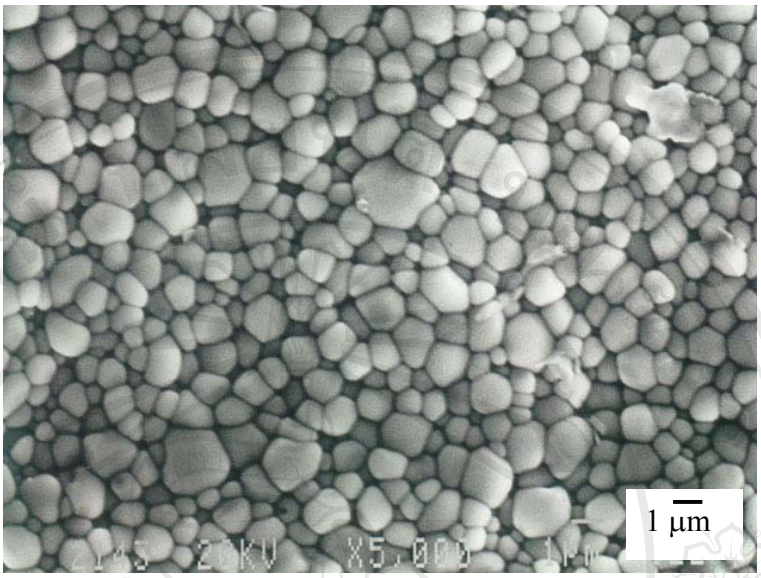

(a)

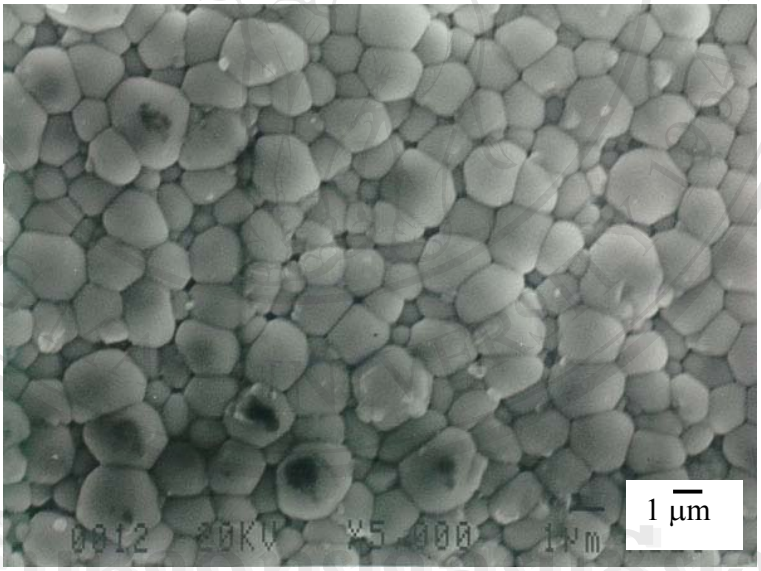

(b)

Figure 4.16 SEM micrographs of as sintered surface of PZT ceramics fabricated from spray dried granules sintered at (a) 1100 °C and (b) 1200 °C.

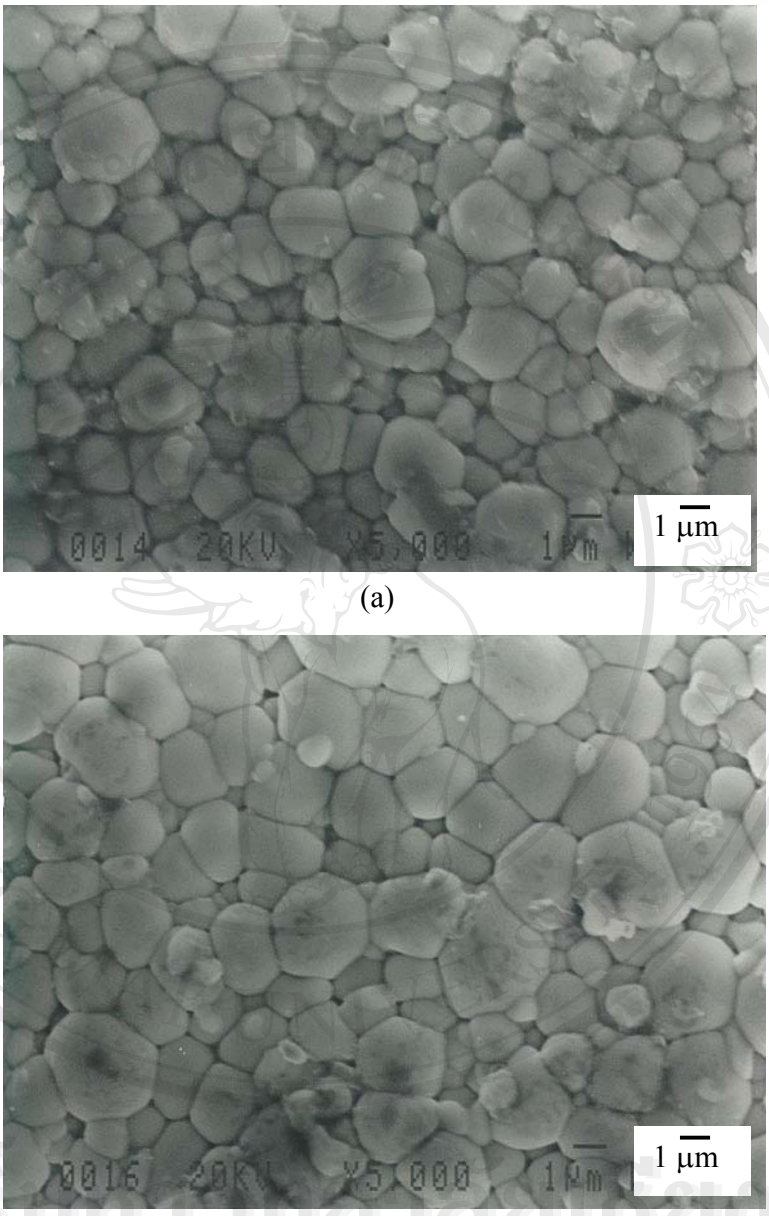

Figure 4.17 SEM micrographs of as sintered surface of PZT ceramics fabricated from spray dried granules sintered at (a) 1230 °C and (b) 1250 °C.

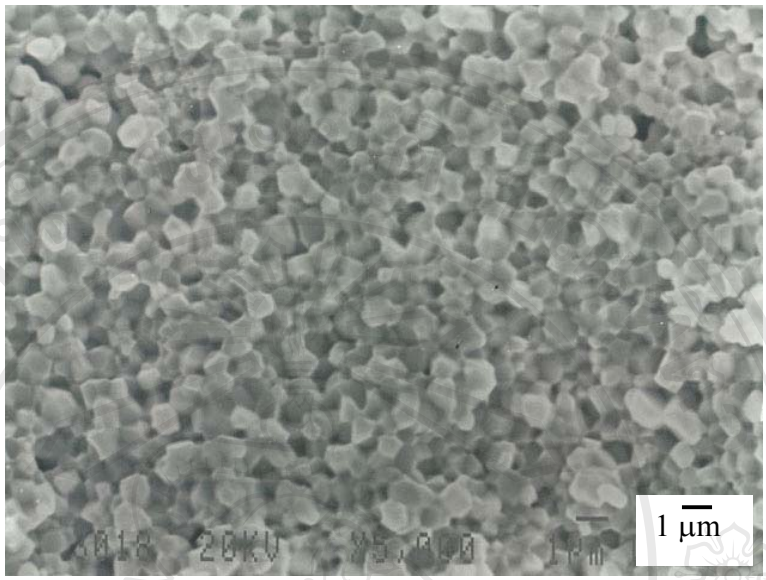

(a)

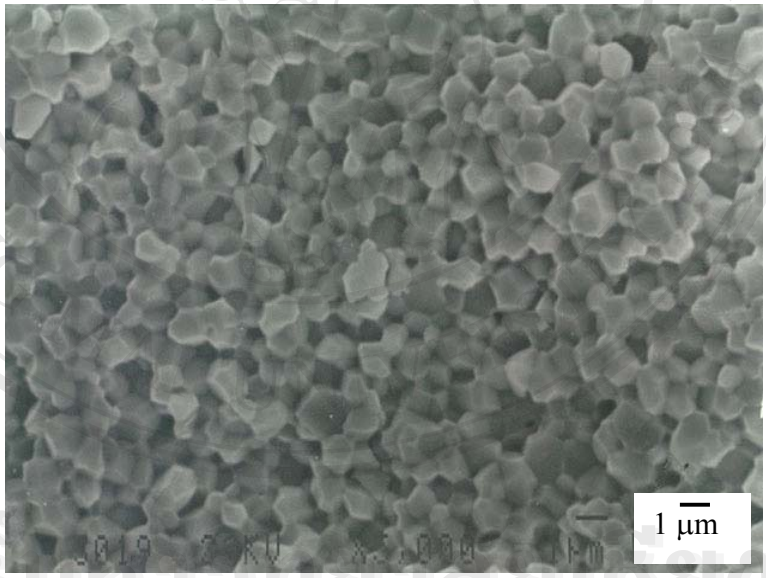

(b)

Figure 4.18 SEM micrographs of fracture surface of PZT ceramics fabricated from spray dried granules sintered at (a) 900 °C and (b) 1000 °C.

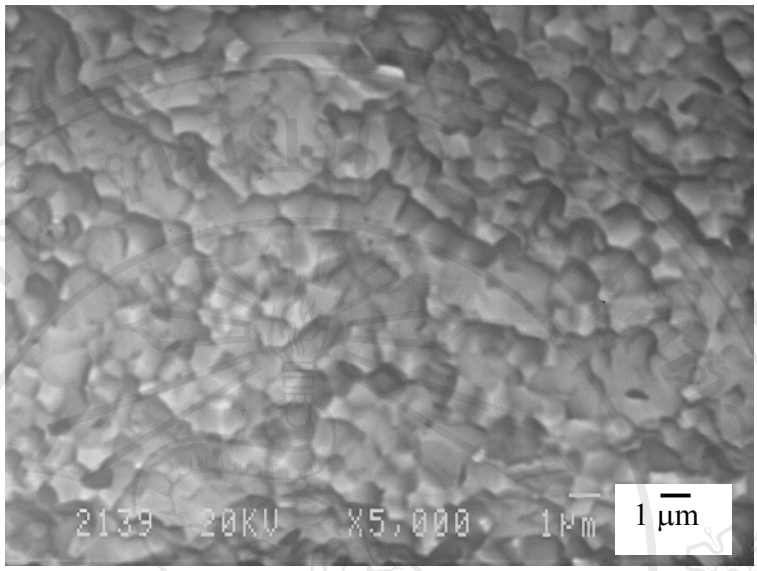

(a)

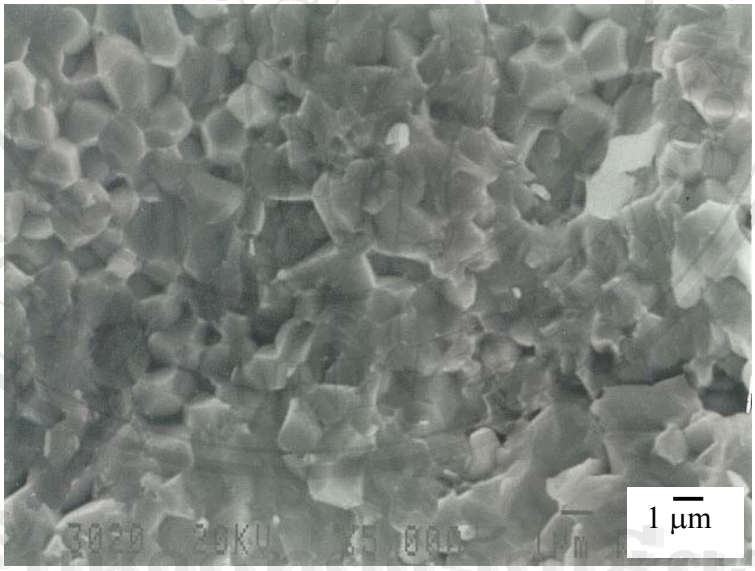

(b)

Figure 4.19 SEM micrographs of fracture surface of PZT ceramics fabricated from spray dried granules sintered at (a) 1100 °C and (b) 1200 °C.

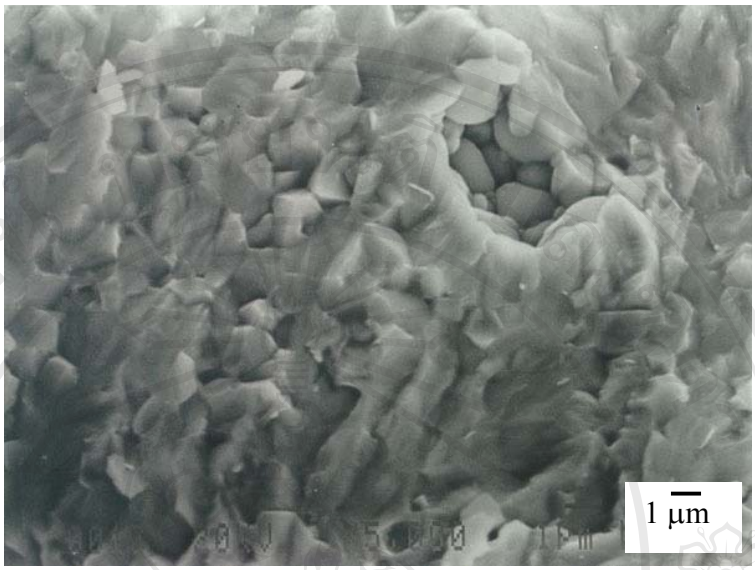

(a)

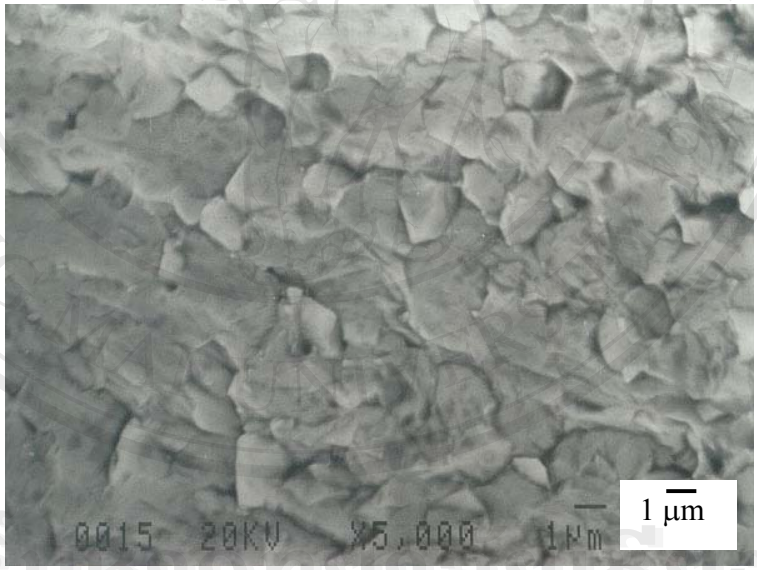

(b)

Figure 4.20 SEM micrographs of fracture surface sprayed of PZT ceramics fabricated from spray dried granules sintered (a) 1230 °C and (b) 1250 °C.

4.2 Characterization of PZT sample made by conventional mixed oxide method

4.2.1 Phase formation of PZT powder

For PZT powder prepared from the conventional mixed oxide method, the X-ray diffractograms of calcined and sintered at different temperatures are shown in Figure 4.21 and Fig. 4.22, respectively. XRD patterns indicate that the PZT phase forms when the calcining temperature is about 800 °C. All the obtained PZT peaks are matched with JCPDS file no. 33-784 [123]. Moreover, a trace of unreacted ZrO_2 was found in the calcined samples, but it was not detected in the sintered samples. Only the single phase of tetragonal perovskite PZT was obtained. The results indicate that the optimize condition for sintering the PZT prepared by mixed oxide method is 1250 °C.

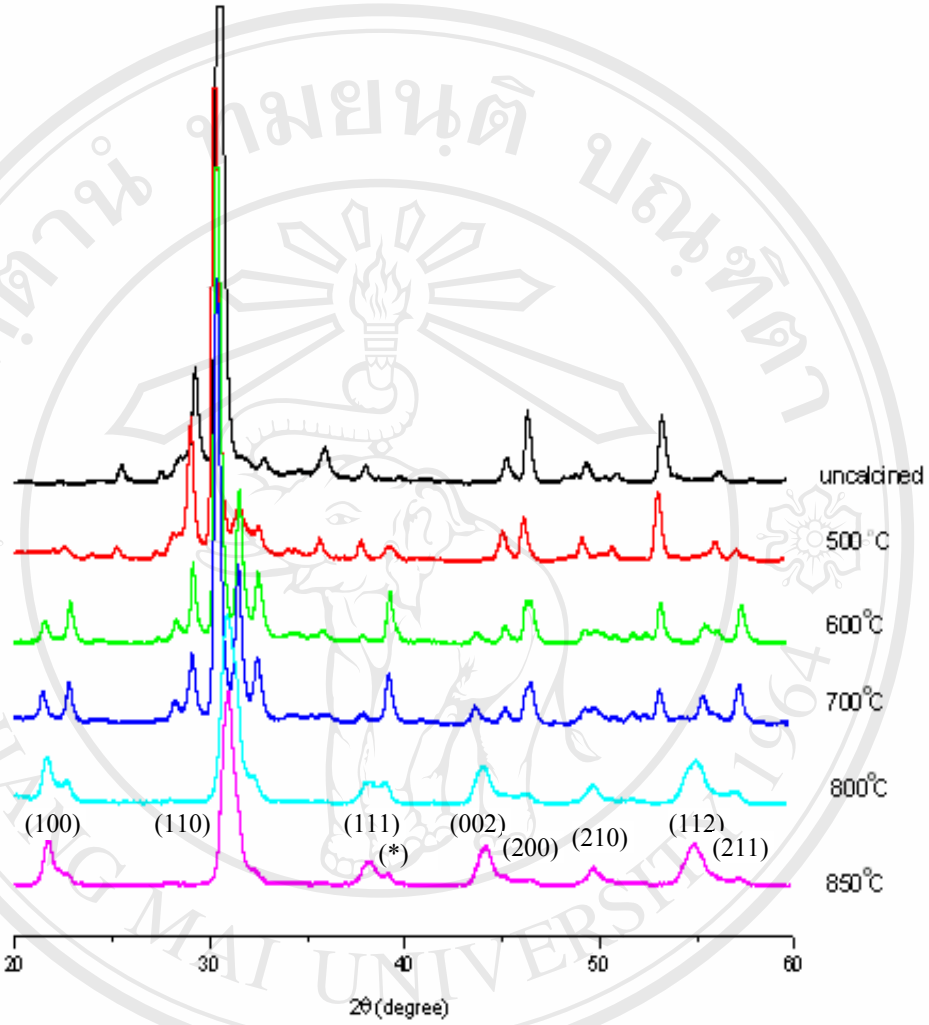

Figure 4.21 XRD patterns of PZT mixed oxide powder calcined with several temperatures. (* is the unreacted ZrO_2)

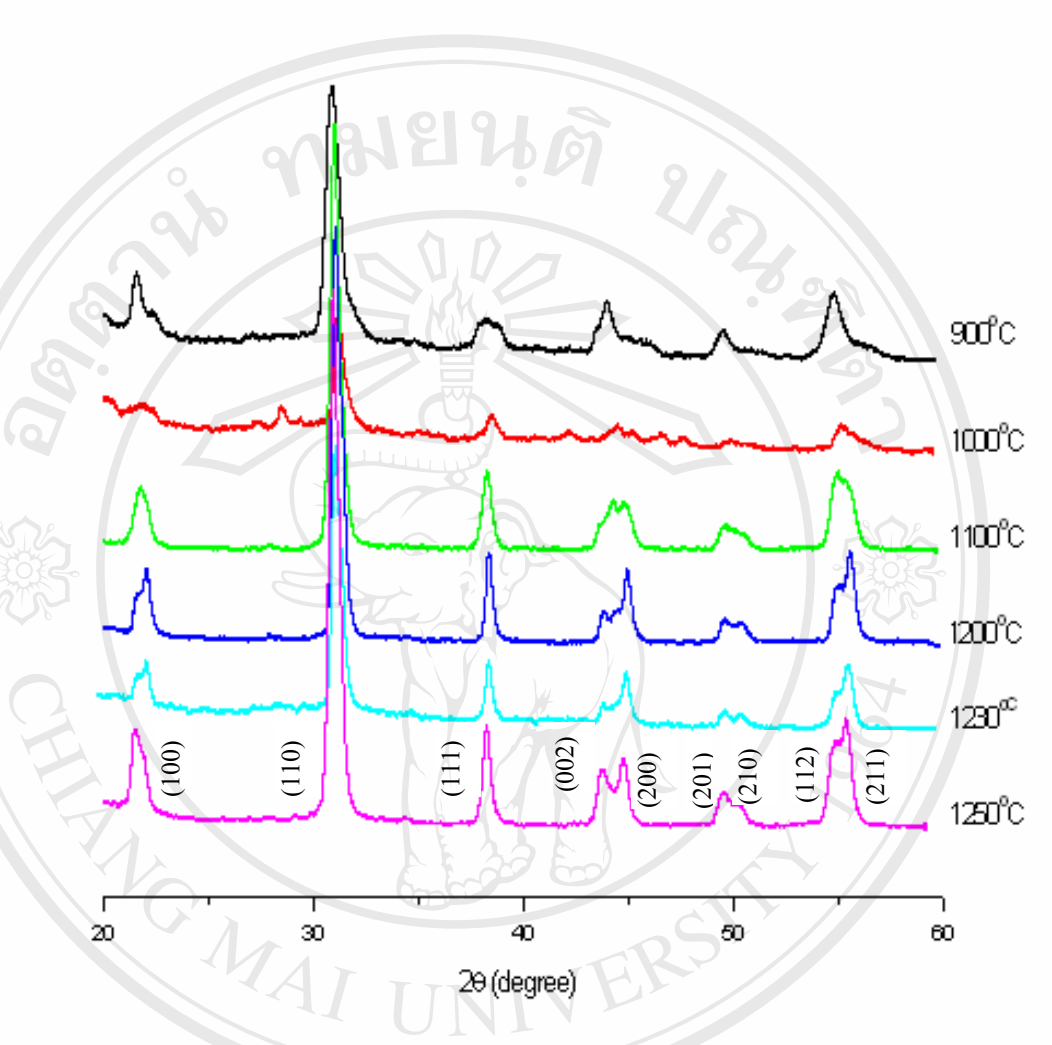

Figure 4.22 XRD patterns of PZT mixed oxide sample sintered with several temperatures.

4.2.2 Investigation of particle size distribution of PZT mixed oxide powder

The distribution of particle size is shown in Figure 4.23-4.25. From the results, it can be seen that the normal distribution of particle size was not obtained and the average size appeared in two ranges which may be due to the effect from the agglomeration of particles. The average particle size of PZT powder prepared by the conventional mixed oxide method is in the range of 2-9 μm which bigger than sprayed powder. Moreover, the trend of average particle size is increased with calcining temperature.

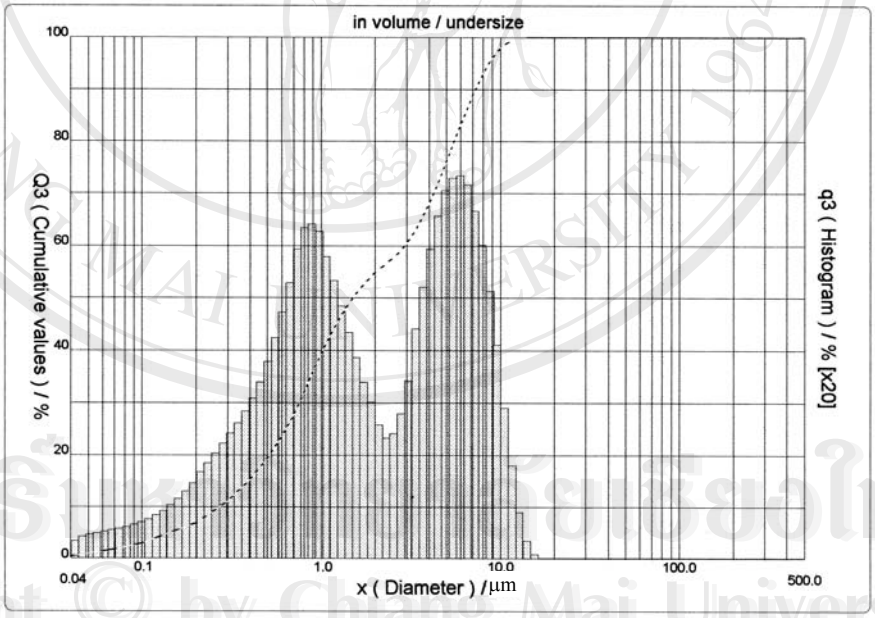

Figure 4.23 The particle size distribution of mixed oxide PZT powder calcined at temperature 500 °C.

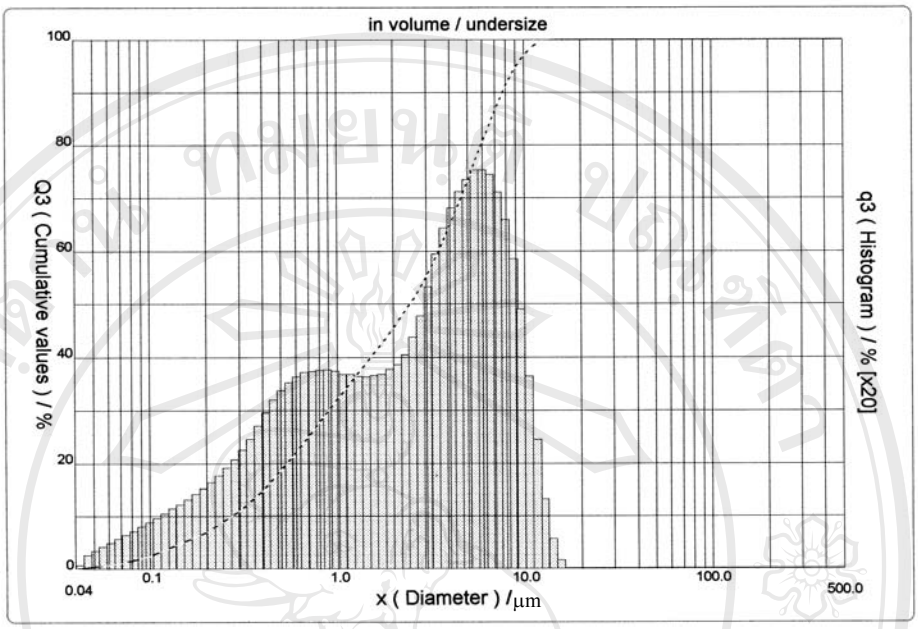

(a)

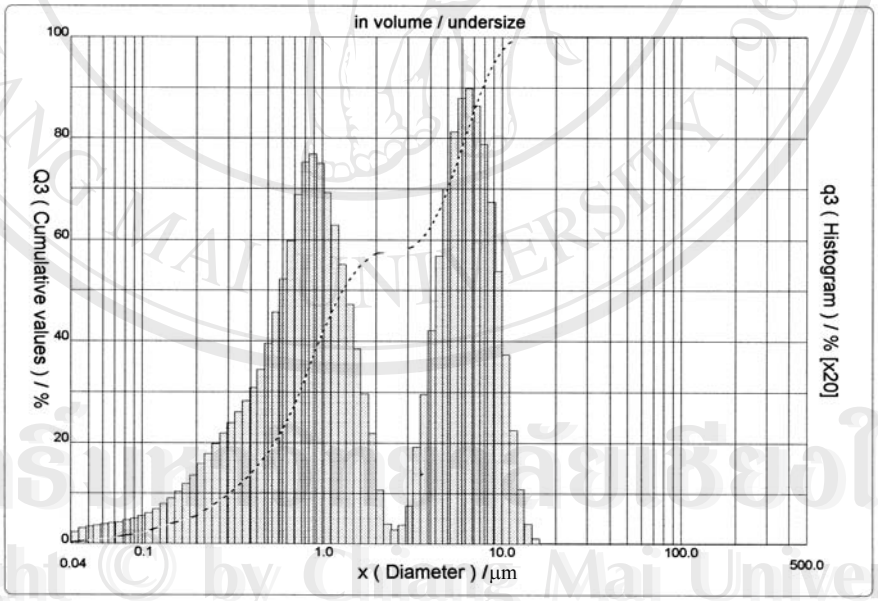

(b)

Figure 4.24 The particle size distribution of mixed oxide PZT powder calcined at temperature (a) 600 °C and (b) 700 °C

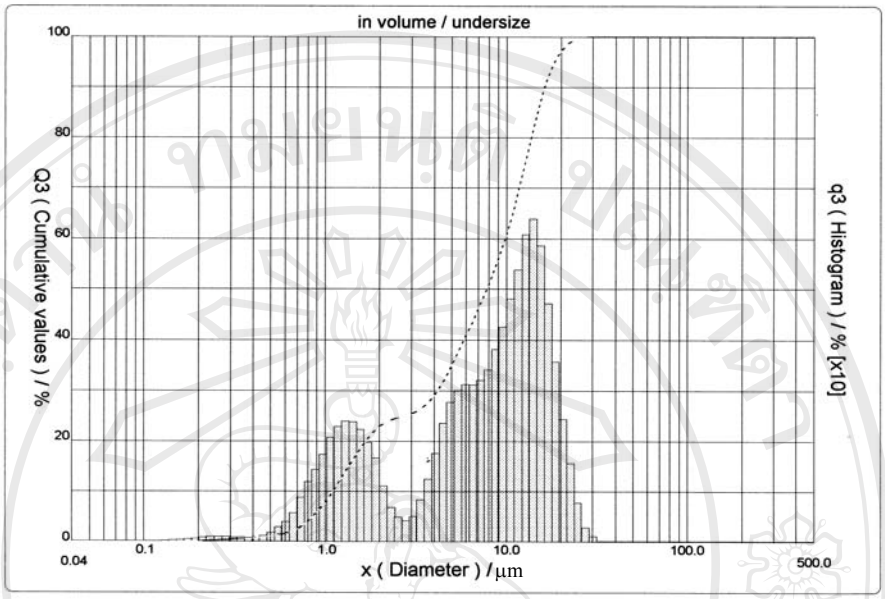

(a)

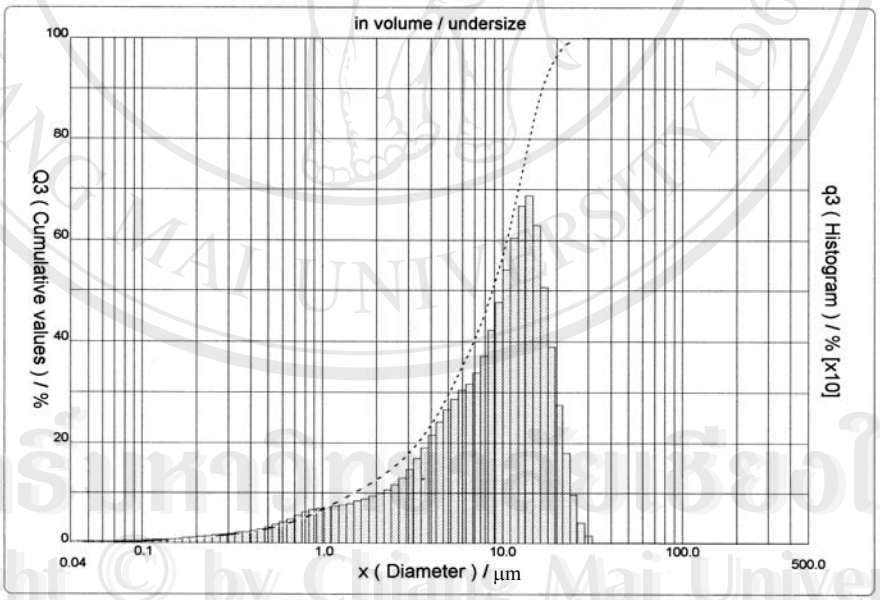

(b)

Figure 4.25 Particle size distribution of mixed oxide PZT powder calcined at temperature (a) 800 °C and (b) 850 °C.

4.2.3 Examination of PZT mixed powder by SEM

The SEM micrographs of PZT powder and ceramics were shown in Figure 4.26-4.28. It can be seen that the morphology of powder obtained from mixed oxide show irregular shape and become bigger when the calcining temperature is higher. The microstructure of the as-sintered and the fracture surface of PZT samples were illustrateded in Figure 4.29-4.31 and Figure 4.32-4.34, respectively. The micrographs show the normal grain growth of particles with the average grain size are in the range of 0.9-2.9 μm for as sintered surface and 1.21-3.40 μm for fracture surface. Moreover, the grain packing of mixed oxide samples are not tight when compared with the spray dried powder which sintered as the same condition.

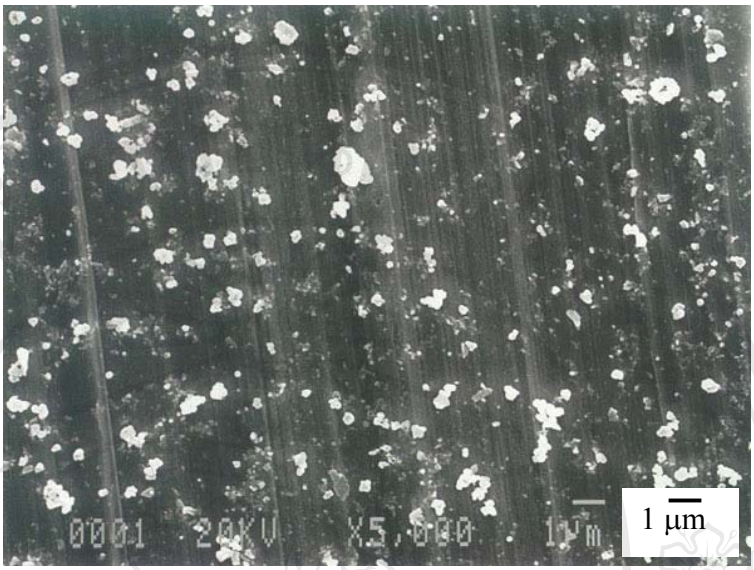

(a)

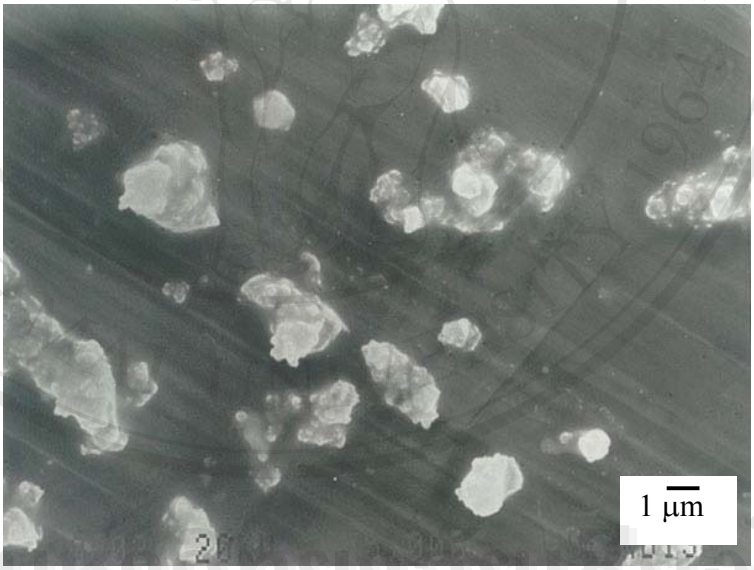

(b)

Figure 4.26 SEM micrographs of mixed oxide powder (a) uncalcined and (b) calcined at 500 ℃.

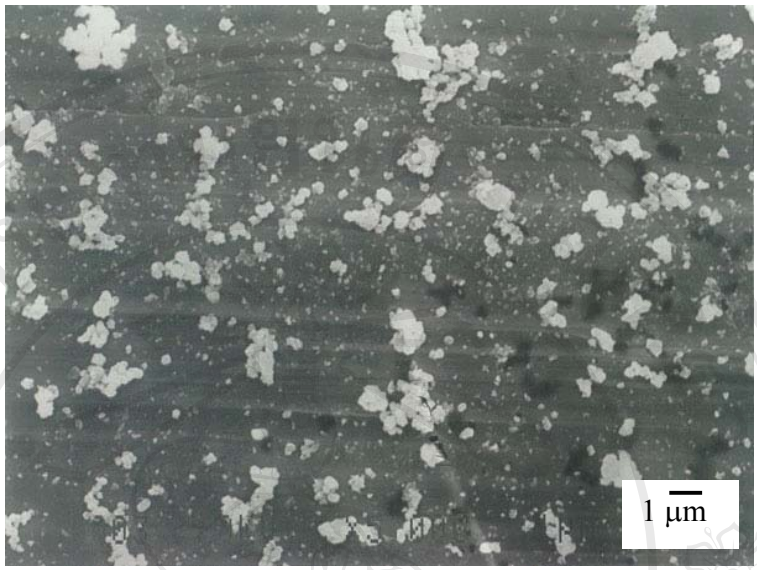

(a)

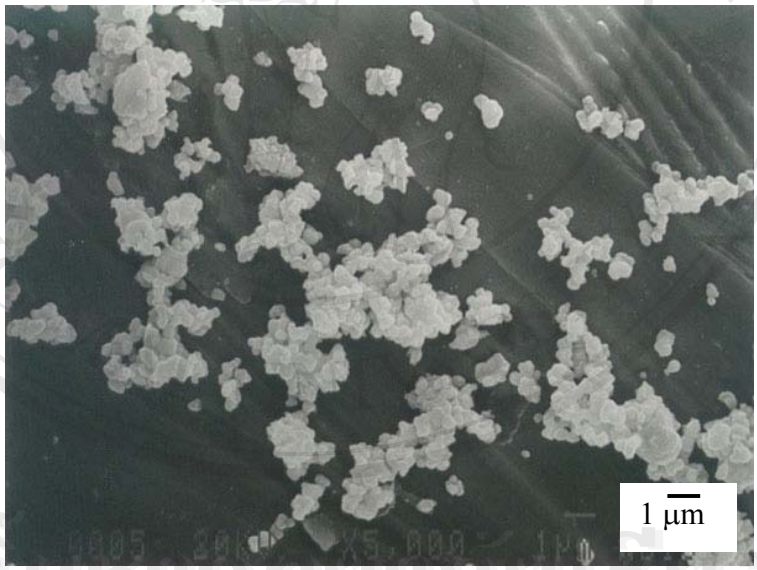

(b)

Figure 4.27 SEM micrographs of mixed oxide powder calcined at (a) 600 °C and (b) 700 °C.

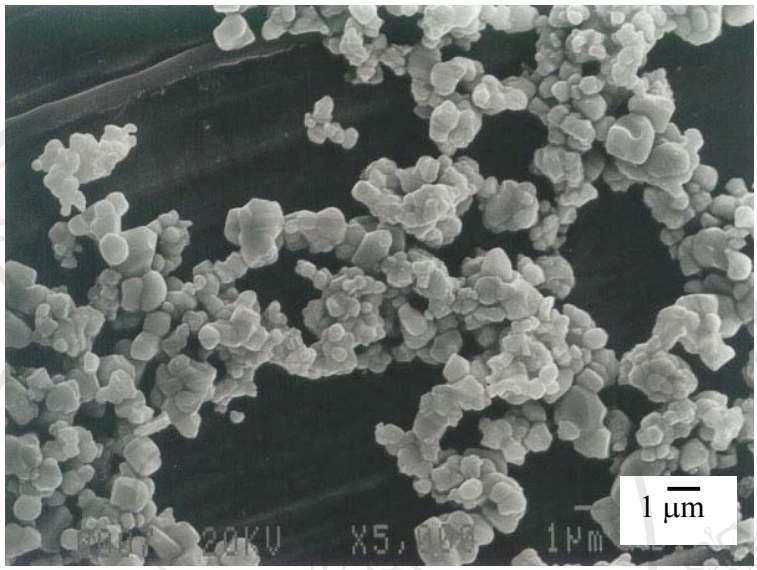

(a)

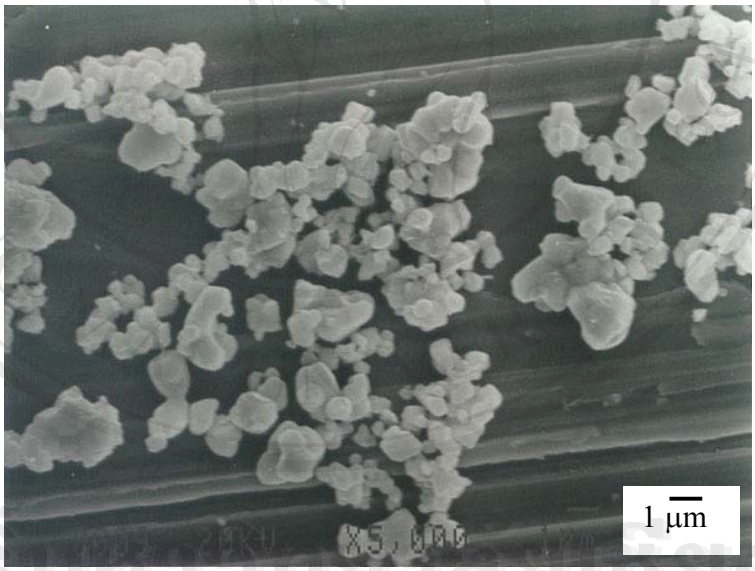

(b)

Figure 4.28 SEM micrographs of mixed oxide powder calcined at (a) 800 °C and (b) 850 °C.

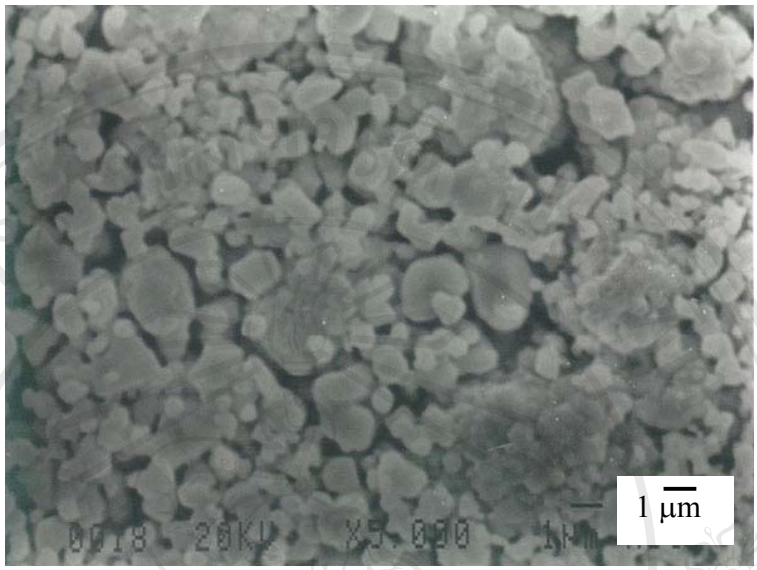

(a)

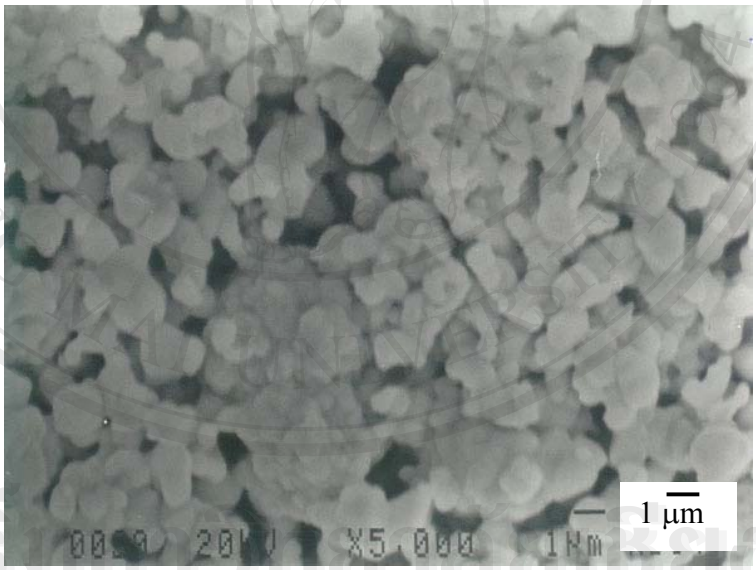

(b)

Figure 4.29 SEM micrographs of as sintered surface of mixed oxide ceramic sintered at (a) 900 °C and (b) 1000 °C.

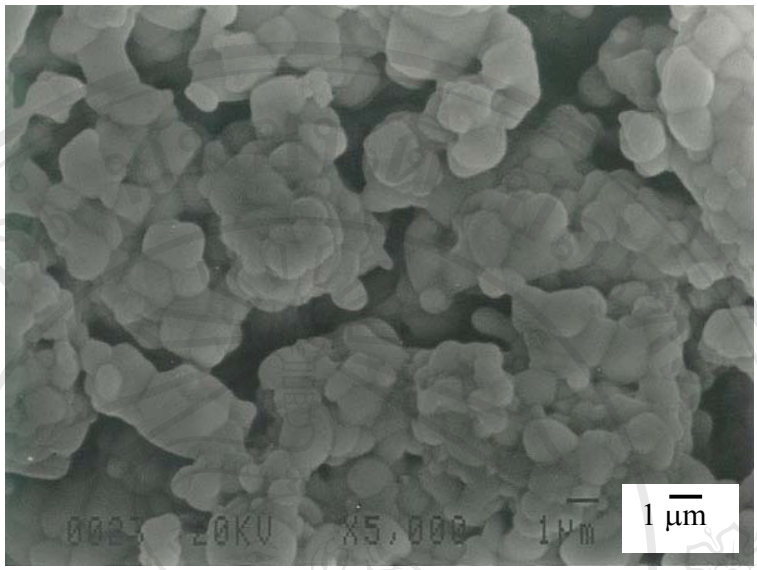

(a)

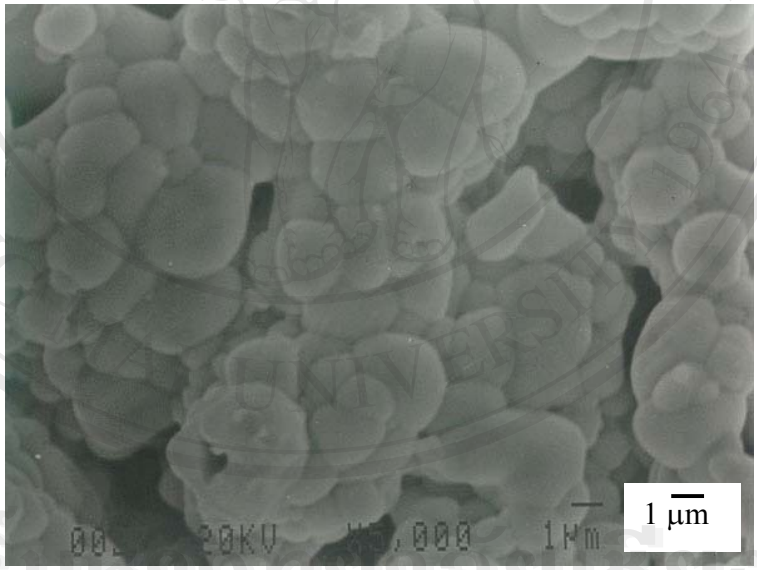

(b)

Figure 4.30 SEM micrographs of as sintered surface of mixed oxide ceramic sintered at (a) 1100 °C and (b) 1200 °C.

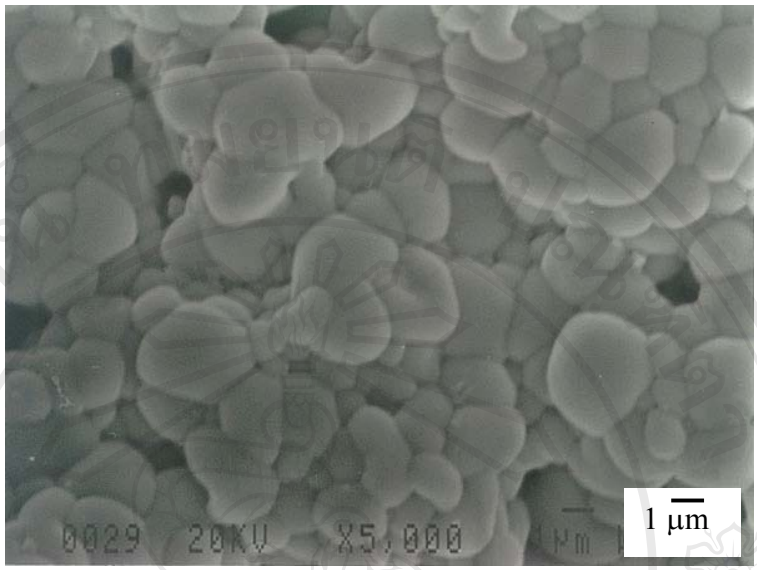

(a)

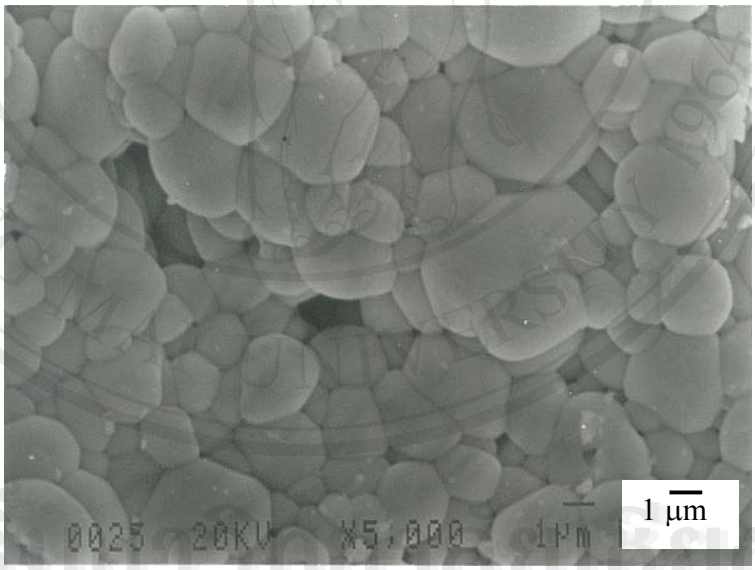

(b)

Figure 4.31 SEM micrographs of as sintered surface of mixed oxide ceramic sintered at (a) 1230 °C and (b) 1250 °C.

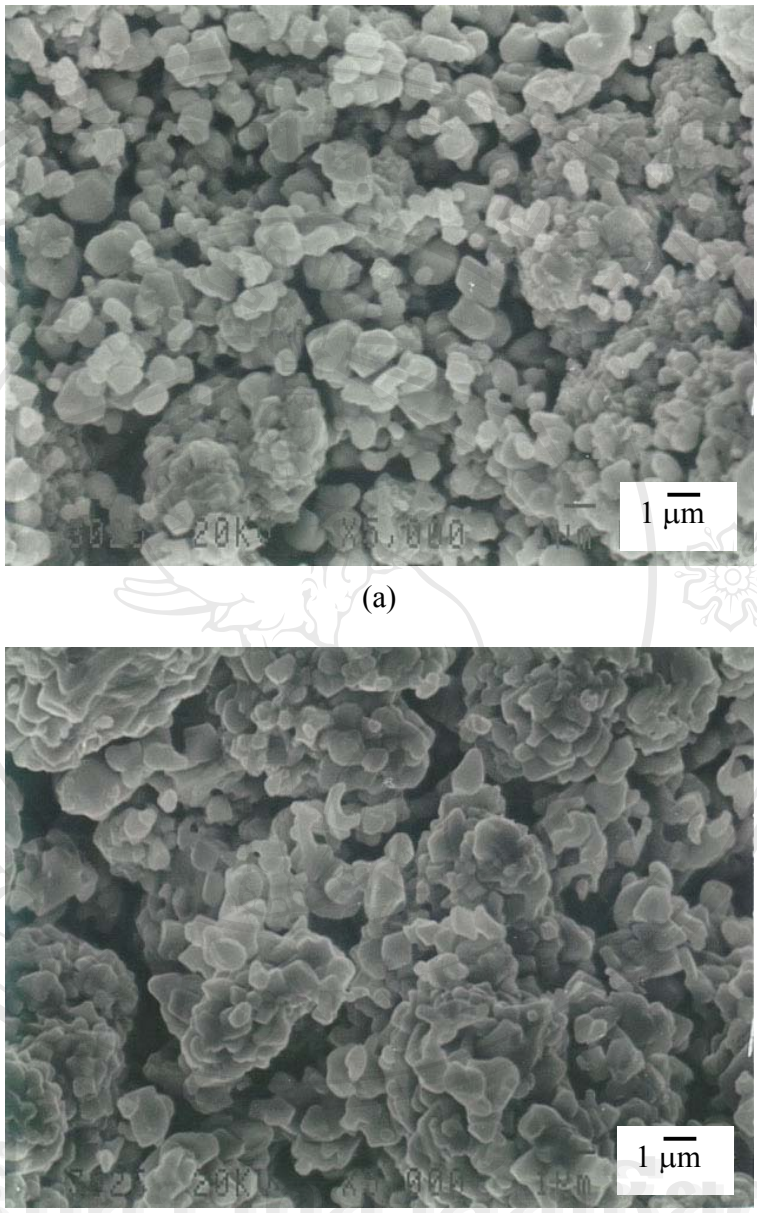

(a)

(b)

Figure 4.32 SEM micrographs of fracture surface of mixed oxide ceramic sintered at (a) 900 °C and (b) 1000 °C.

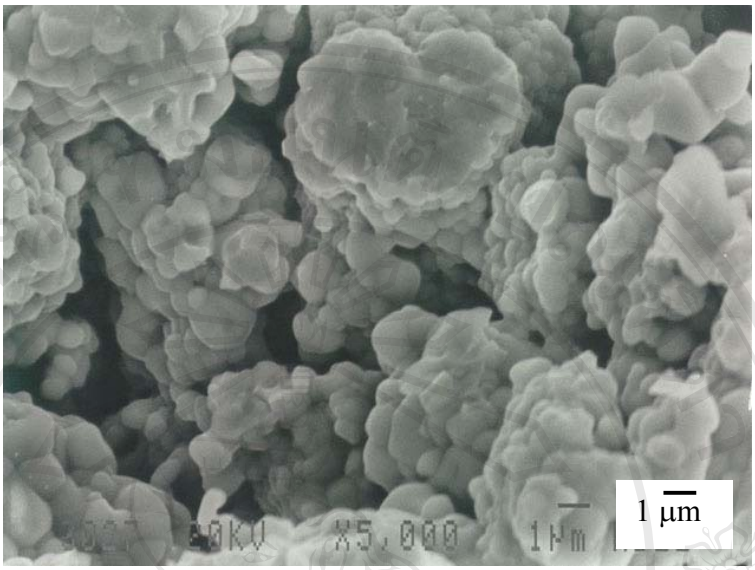

(a)

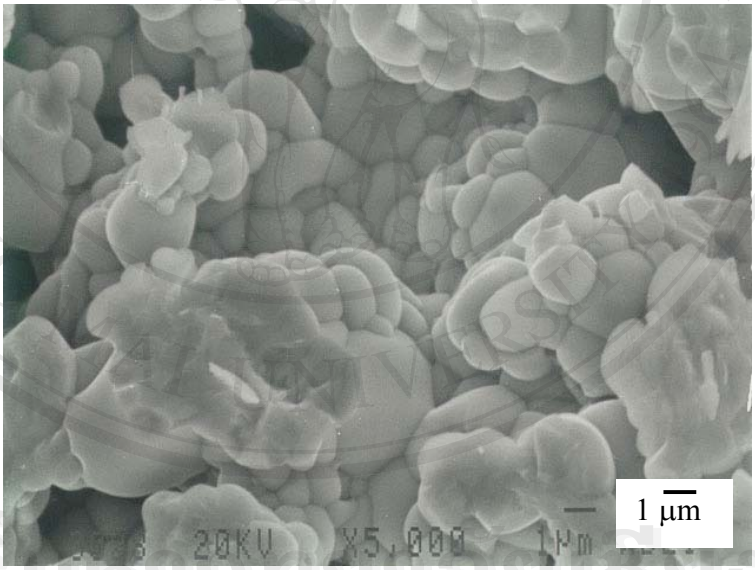

(b)

Figure 4.33 SEM micrographs of fracture surface of mixed oxide ceramic sintered at (a) 1100 °C and (b) 1200 °C.

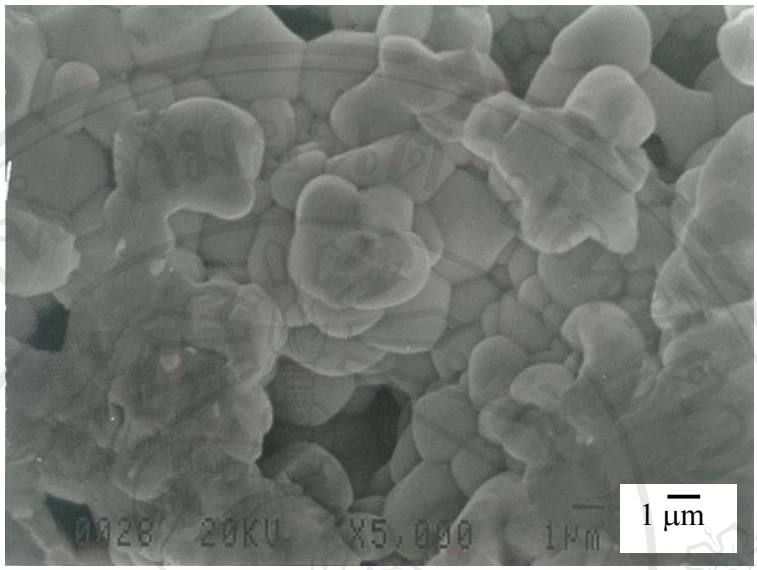

(a)

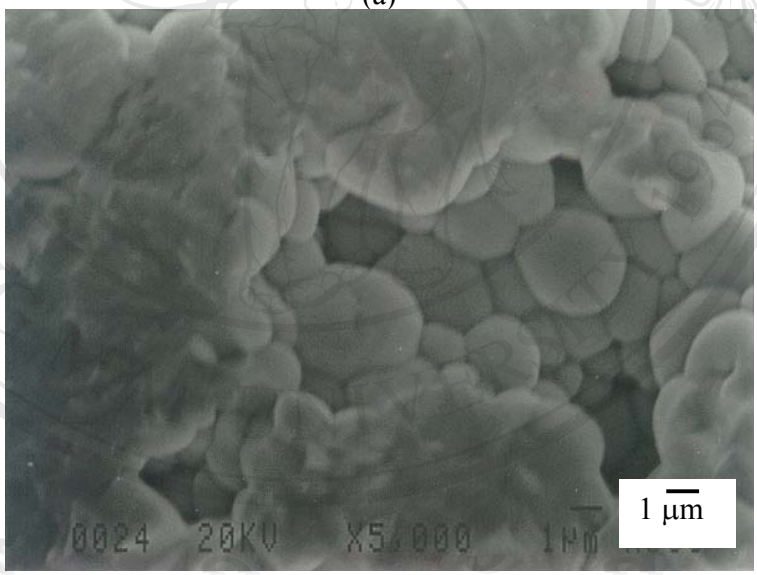

(b)

Figure 4.34 SEM micrographs of fracture surface of mixed oxide ceramic sintered at (a) 1230 °C and (b) 1250 °C.

4.3 Characterization of modified PZT sample

By the modify method, sample powder made by spray dry technique was mixed with MnO_2 through wet-milling method. The corresponding Mn-doped PZT ceramics were obtained via the conventional solid state method.

4.3.1 Phase transformation of modified PZT ceramics

From the XRD, it can be seen that the modified ceramics exhibit tetragonal PZT phase when sintering temperature is higher than 900 °C. The unidentified phase was observed in PZT. However, trend of the second phase intensity shows lower when sintering temperature is increased.

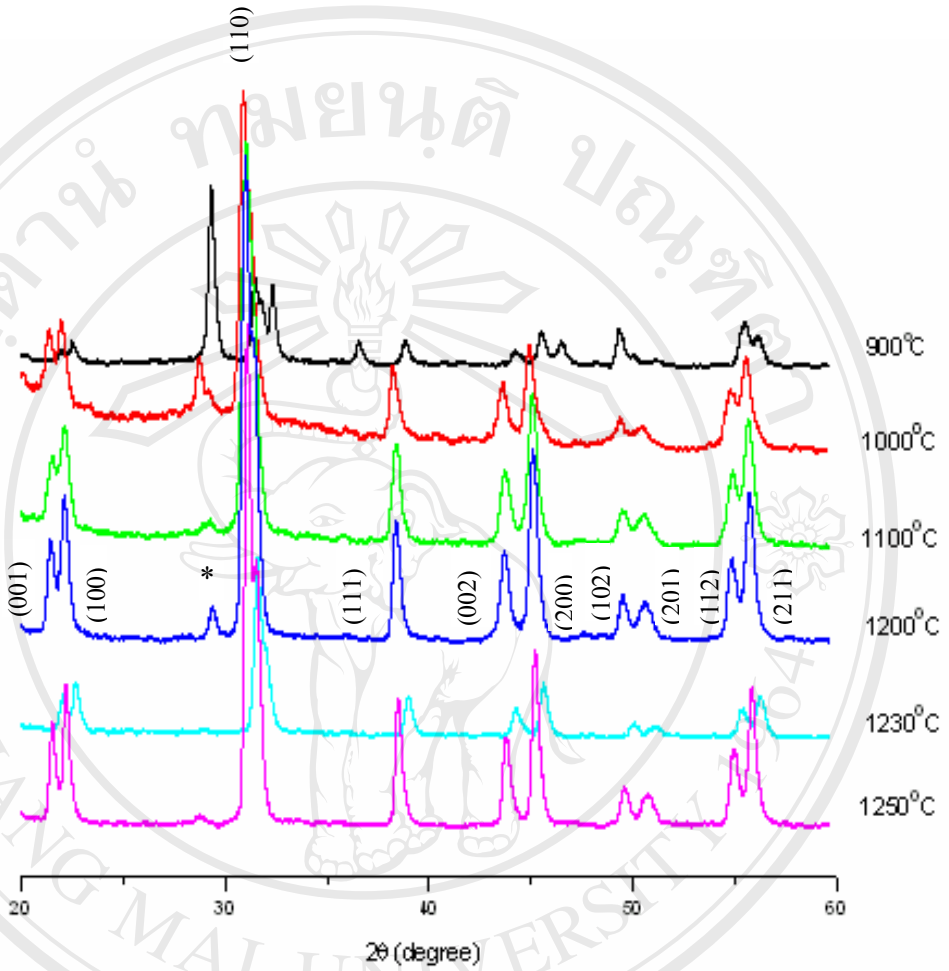

Figure 4.35 XRD patterns of PZT modified ceramics sintered at several temperatures. (* is the unidentified phase)

4.3.2 Microstructure of modified PZT

SEM micrographs of as sintered and fracture surface of modified PZT ceramics are shown in Figure 4.36-4.38 and Figure 4.39-4.41, respectively.

It can be concluded that the irregular shape of grain was observed and became more spherical shape when sintering temperature was higher than 1000 °C. Grains grew bigger with the sintering temperature. However, the SEM of ceramics sintered at 1250 °C show not good surface. It may be due to the effect of over sintering.

For the fracture surface, it can be seen that the polyhedral shape show up in the sample as sintered 900 °C. The grain packing of samples are more tightly when sintering temperature is increased. However, the large pores appear in the grain.

The average grain size of sample are in the range of 1.22-2.86 μm and 1.16-2.88 μm for as sintered and fracture surfaces, respectively.

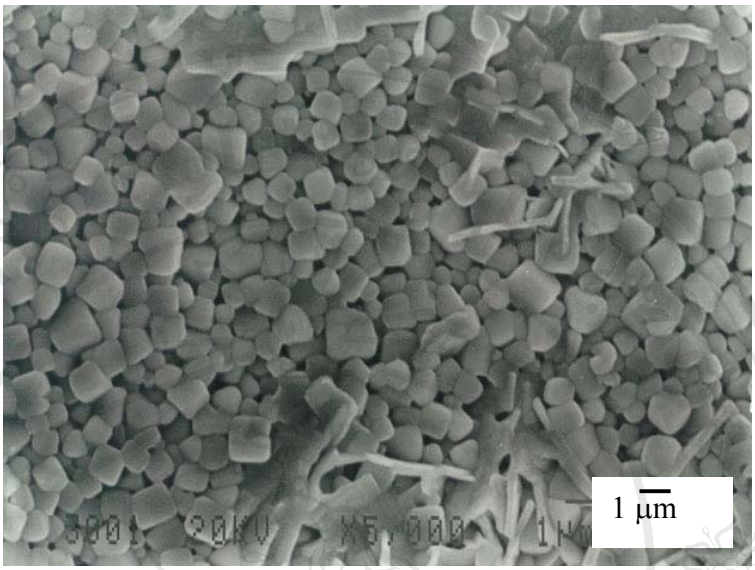

(a)

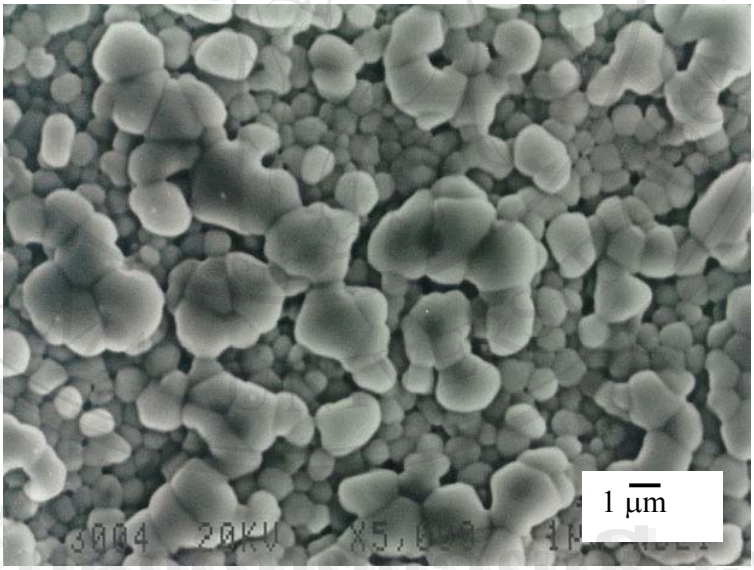

(b)

Figure 4.36 SEM micrographs of the as sintered surface of modified ceramics sintered at (a) 900 °C and (b) 1000 °C.

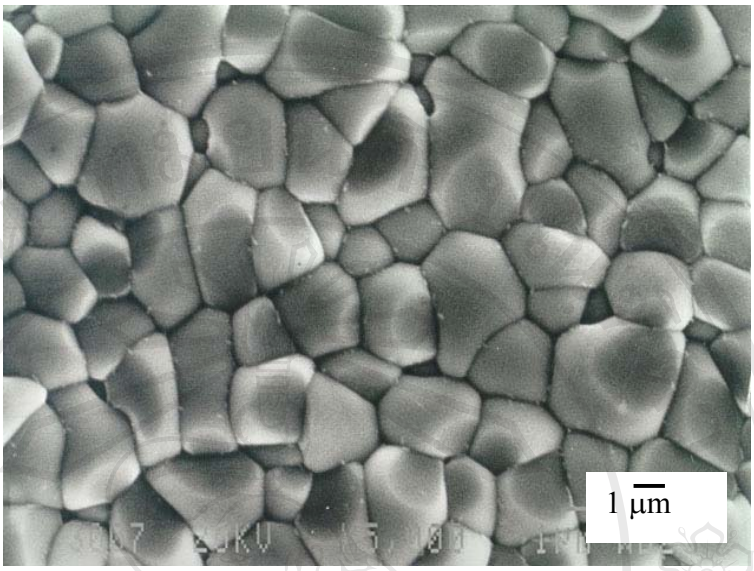

(a)

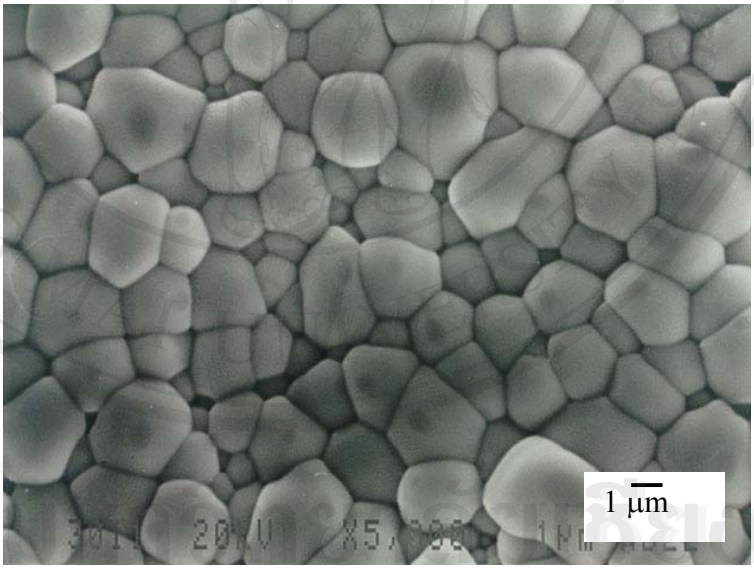

(b)

Figure 4.37 SEM micrographs of the as sintered surface of modified ceramics sintered at (a) 1100 °C and (b) 1200 °C.

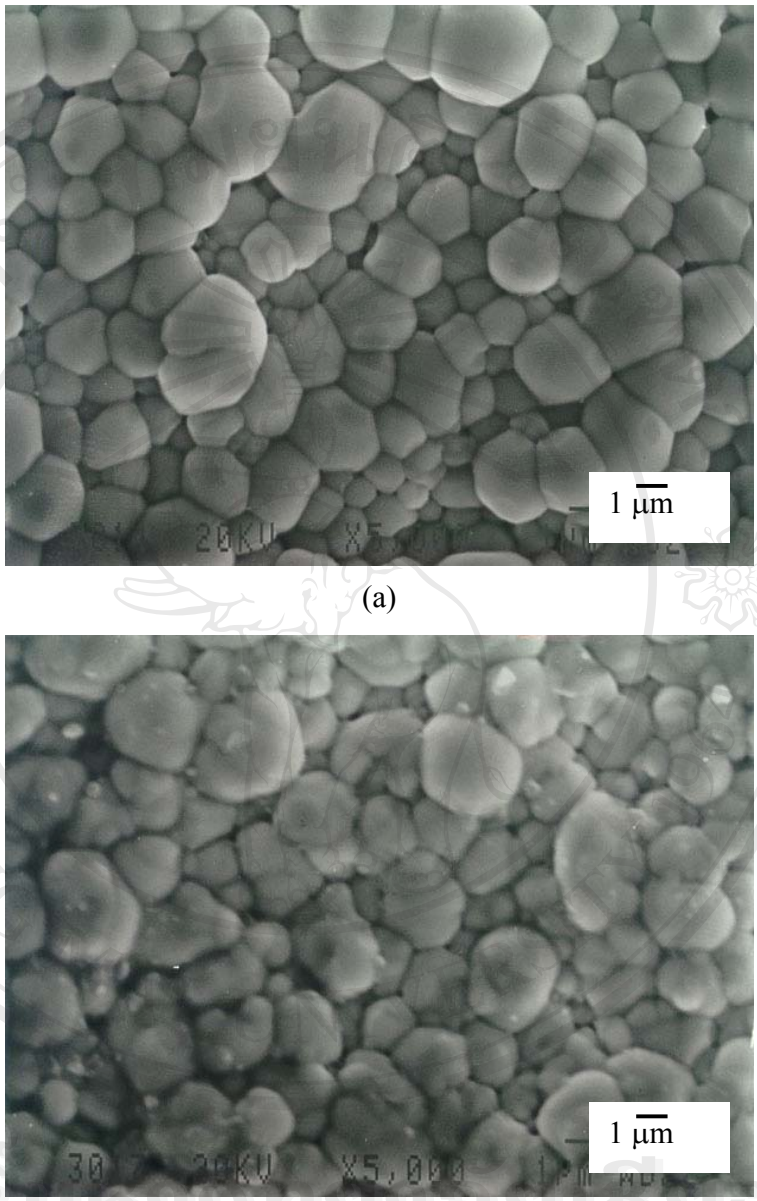

(a)

(b)

Figure 4.38 SEM micrographs of the as sintered surface of modified ceramics sintered at (a) 1230 °C and (b) 1250 °C.

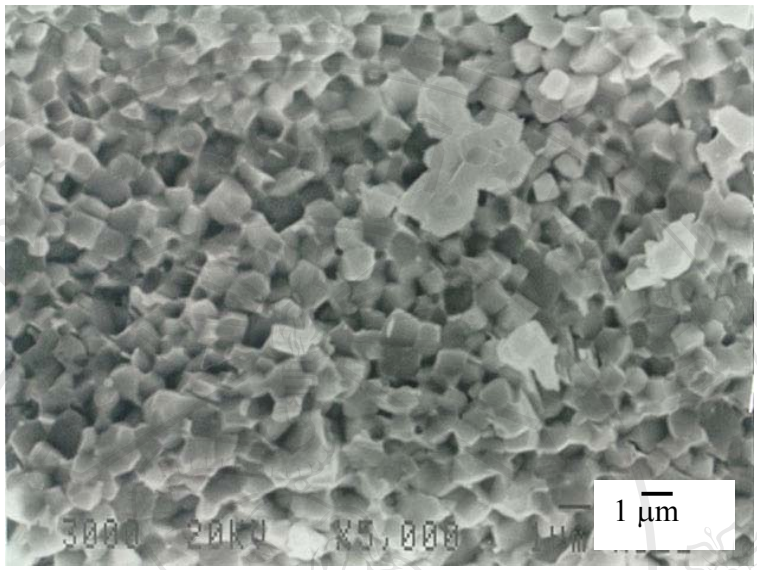

(a)

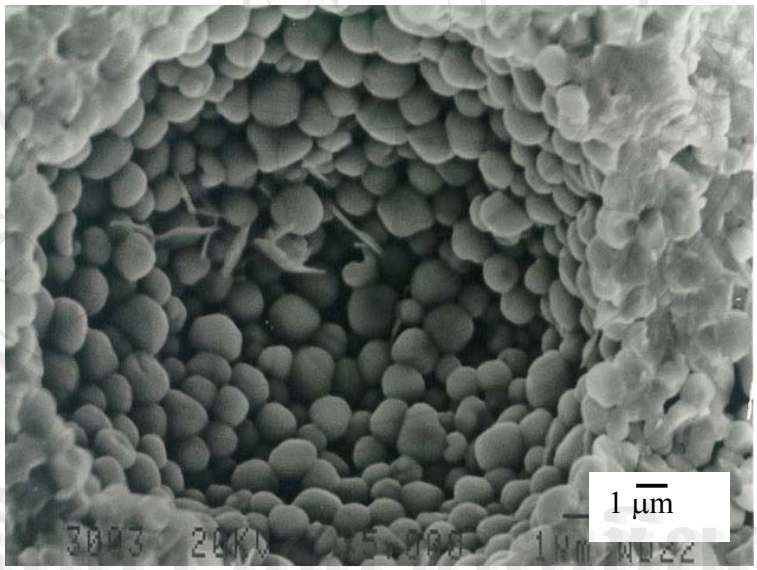

(b)

Figure 4.39 SEM micrographs of the fracture surface of modified ceramics sintered at (a) 900 °C and (b) 1000 °C.

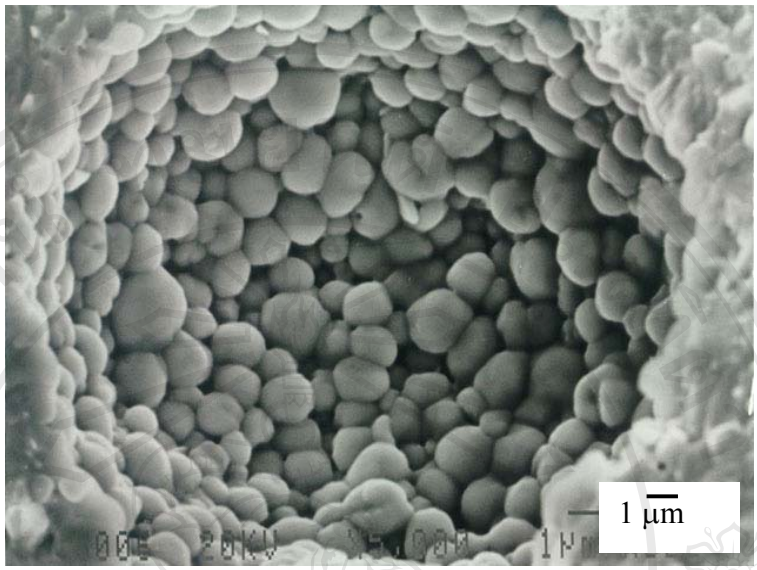

(a)

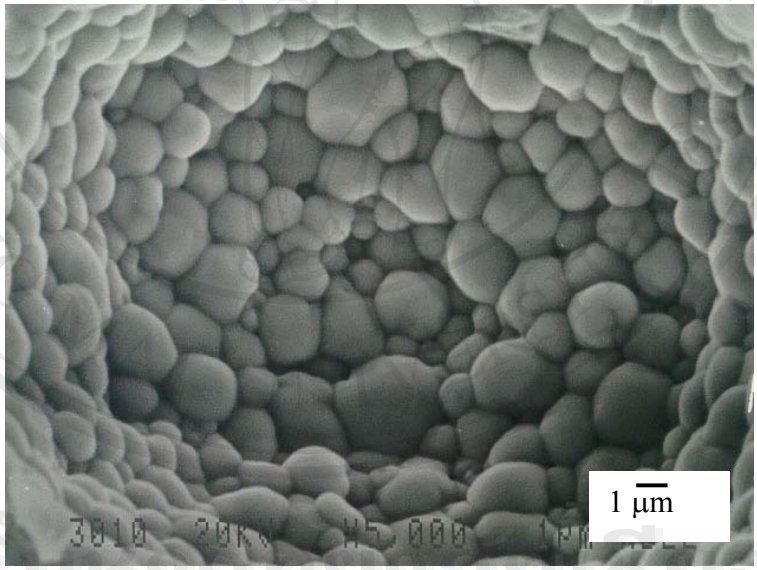

(b)

Figure 4.40 SEM micrographs of the fracture surface of modified ceramics sintered at (a) 1100 °C and (b) 1200 °C.

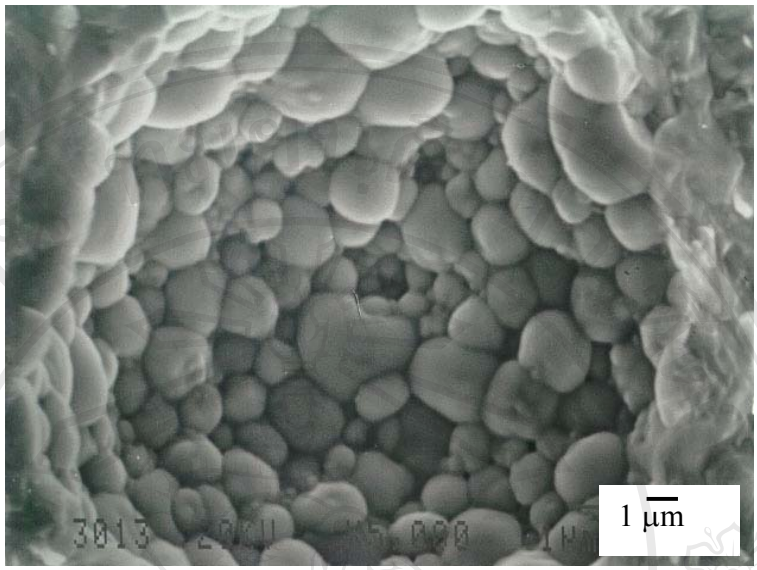

(a)

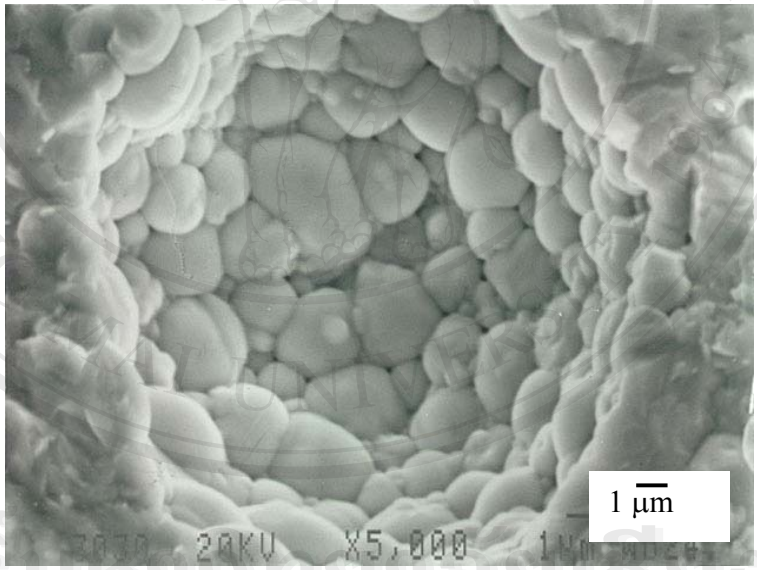

(b)

Figure 4.41 SEM micrographs of the fracture surface of modified ceramics sintered at (a) 1230 °C and (b) 1250 °C.

4.4 Physical properties of PZT ceramics

The physical properties of PZT ceramics such as shrinkage, porosity and density of PZT ceramics were investigated and shown in Table 4.2. From Table 4.2, it can be concluded that mixed oxide samples sintered at 900-1100 °C could not be measured these properties since the sintering temperature is improper and it is high enough for packing the grain. These have the effect to the strength of ceramic samples. However, ceramics become more strength when sintering temperature is increasing (1200-1250 °C). Value of shrinkage, porosity and density are in the range of 1.02-5.58%, 26.09-11.86% and 5.99-7.06 g/cm^3, respectively. For sprayed and modified ceramics, the physical properties are 20.71-22.15%, 2.08-4.49% and 7.65-7.82 g/cm^3 and 13.05-15.23%, 9.86-19.10% and 6.48-7.22 g/cm^3.

For ceramics employing the sprayed dried powder sample, it can be concluded that the ceramic sintered at 1000 °C has the highest density (about 7.82 g/cm^3 or 97 % of theoretical density) which is closed to that obtained by Tunkasiri [26], who however used the high-quality and high cost chemicals. The density of the ceramics was found to increase as the temperature rises up to 1000 °C and gradually decreases with the increasing temperature. This is probably owing to the lead loss that normally occurs at the high sintering temperature thus resulting in decrease of the shrinkage and porosity of the ceramics.

The optimize conditions 1250 °C, 1000 °C and 900 °C for mixed oxide sample, sprayed ceramics and modified ceramics, respectively.

4.5 Dielectric and piezoelectric properties of PZT ceramics

The piezoelectric, dielectric and physical properties of PZT ceramics from spray drying, mixed oxide and modified methods are shown in Table 4.3, Table 4.4 and Table 4.5, respectively.

The dielectric constant (ε_r) and the planar coupling constant (d_{33}) of the ceramics employing the sprayed dried granules were tabulated in Table 4.3 together with those of Tunkasiri [26], Lal *et al*. [127] and Zhilun *et al*. [128]. The values of the dielectric constant, with the maximum of 780 obtained from the ceramics sintered at 1100 °C, fall pretty well between those of the previous work [99,111,113]. The tanδ, d_{33} and k_p values of our results are in the ranges of 0.004 to 0.02, 130 to 168 pC/N and 0.52 to 0.60 respectively. These are comparable to those obtained by Lal *et al*. [127], Tunkasiri [26] and Zhilun *et al*. [128], though the former two used the high purity chemicals for their preparations and the latter employed mixed oxide route plus low melting frit.

The ε_r, d_{33} and k_p values of PZT ceramics made from conventional method were shown in Table 4.4. The ε_r, d_{33} and k_p are 108-806, 57-306 pC/N and 0.25-0.64, respectively.

The dielectric and piezoelectric properties of modified ceramics are shown in Table 4.5. It can be seen that samples show the dielectric constant of 579-1561, d_{33} values of 15-100 pC/N and the k_p is in the range of 0.26-0.37.

Table 4.3 Dielectric and piezoelectric properties of the PZT ceramics produced from the spray dried granules.

Sintering temperature (^oC)	**Dielectric constant (ε_r)**	**Loss angle (tanδ)**	**k_p**	**d_{33} (pC/N)**
900	675	0.02	0.54	136
960 [126]	1100	0.008	0.57	250
1000	690	0.001	0.60	168
1050 [26]	490	0.001	0.44	-
1100	780	0.002	0.52	130
1200	675	0.004	0.60	156
1200 [127]	1180	0.007	0.45	230
1250	630	0.002	0.58	153

Table 4.4 Dielectric and Piezoelectric properties of the PZT ceramics produced from the mixed oxide powder.

Sintering temperature (^oC)	**Dielectric constant (ε_r)**	**Loss angle (tanδ)**	**k_p**	**d_{33} (pC/N)**
900	108	0.18	0.33	57
1000	218	0.06	0.32	95
1100	283	0.01	0.25	172
1200	504	0.01	0.41	240
1230	627	0.01	0.51	264
1250	806	0.01	0.64	306

Table 4.5 Piezoelectric, dielectric and physical properties of the PZT ceramics produced from the mixed oxide powder.

Sintering temperature (^oC)	**Dielectric constant (ε_r)**	**Loss angle (tanδ)**	**k_p**	**d_{33} (pC/N)**
900	859	0.21	0.26	15
1000	1561	0.5	0.31	97
1100	691	0.1	0.37	72
1200	605	0.01	0.34	77
1230	583	0.01	0.34	68
1250	579	0.01	0.34	100

4.6 Properties of Piezoceramic-Polymer Composites

4.6.1 Physical properties

The volumetric percentage of density (ρ) and acoustic impedance (Z) of the composites are tabulated in the Table 4.6 with those obtained by others [129-132] The density of all composite samples were measured using Archimedes principle and the volumetric fraction of PZT particles in composites were measured using Equation (3.2).

It can be seen that PZT/epoxy produced from PZT powder of smaller particle size (PZT(sp)/epoxy resin) yields higher volumetric percentage (37%) and possesses higher ρ (2119.6 kg/m^3) and Z (4.84 Mrayls) values as compared to the PZT(m)/epoxy resin composite with corresponding values of 34%, 1878.6 kg/m^3 and 4.12 Mrayls respectively. Both composites fabricated by our methods (combination of suction, dice and fill) were noted to have very low acoustic impedance (4.12 and 4.84 Mrayls) and very close to that of water (1.5 Mrayls). These values are lower than those previously been reported by Nhuapeng and Tunkasiri [129], Sripada *et al*. [130], Grewe *et al*. [131] and Slayton and Setty [132]. This is due to the different of fabrication routes and different volumetric percentages.

Table 4.6 Physical and mechanical properties of the PZT/polymer compositesPZT(m), PZT(sp) = powders obtained from mixed oxide method and spray drying techniques, respectively.

composites	Vol(%)	Density (kg/m^3)	Z (Mrayls)
PZT(m)/epoxy resin	34	1878.6	4.12
PZT(sp)/epoxy resin	37	2119.6	4.84
PZT4040/epoxy resin	33	1822.7	4.39
PZT(m)+Nd/epoxy resin	36	2080.5	4.56
Nhuapeng and Tunkasiri [129]	60	5026	11.41
Sripada *et al*. [130]	-	4225.4	13.94
Grewe *et al*. [131]	40	-	7.50
Slayton and Setty [132]	70	-	8.00

4.6.2 Dielectric Properties and Piezoelectric Properties

Table 4.7 shows dielectric properties (ε_r and tanδ) and piezoelectric properties (d_{33} and k_p) of the composites, together with those of Nhuapeng and Tunkasiri [129], Sripada *et al*. [130], Shrout *et al*. [133], Ohara *et al*. [134], Schwarzer and Roosen [135], Janas *et al*. [136], McNulty *et al*. [137], and Taunaumang [138].

The d_{33} and k_p values obtained from PZT(m)/epoxy composite are 25.3 pC/N and 0.61 respectively. While the d_{33} and k_p values of PZT(sp)/epoxy composite are 20.2 pC/N and 0.54 respectively. It can be seen that the d_{33} values for both composites are very close to the values reported by Nhuapeng and Tunkasiri [129] who fabricated the 0-3 PZT/polymer composites by centrifuge method. The ε_r values obtained from this work is quite low (14-20) which may be due to the effect of quantity of PZT particles in the composites.

Table 4.7 Dielectric and piezoelectric properties of the PZT/polymer composites compared with those of previous work.

composites	d_{33} (pC/N)	k_p	ε_r	tanδ
PZT(m)/epoxy resin	25.3	0.61	14	0.026
PZT(sp)/epoxy resin	20.2	0.54	15	0.05
PZT4040/epoxy resin	35.3	0.56	16	0.03
PZT(m)+Nd/epoxy resin	28.1	0.53	20	0.035
Nhuapeng and Tunkasiri [129]	26	-	84	0.0141
Sripada *et al*. [130]	-	0.4	-	-
Shrout *et al*. [133]	270	-	480	0.017
Ohara *et al*. [134]	274	-	536	-
Schwarzer and Roosen [135]	466	0.58	1146	0.028
Janas *et al*. [136]	370	-	300	0.029
McNulty *et al*. [137]	230	-	130	-
Taunaumang *et al*. [138]	29.6	-	-	-

4.7 Scanning Electron Micrographs of Composites

The top view photograph of the composite is shown in Figure 4.42 and Figure 4.43, shows a typical SEM micrograph of the top view of the composite (combined 0-3 and 1-3 connectivities). Particles obtained from both preparation techniques, were found to have similar morphology. The dark area belongs to the resin while the brighter squares belong to the (0-3) composites. Enlarged pictures of some squares are shown in Fig. 4.44. It can be concluded that the average size of the powders obtained from mixed oxide route is bigger (~ 4 μm) than that obtained from the spray drying technique (~ 1 μm). This is confirmed by the cross section micrographs (Fig. 4.45). However, in Fig. 4.44 the PZT phase shows agglomeration of the particles produced from the spray drying technique. The composites fabricated by suction, dice and fill method leads to a very low acoustic impedance of 4-5 Mrayls.

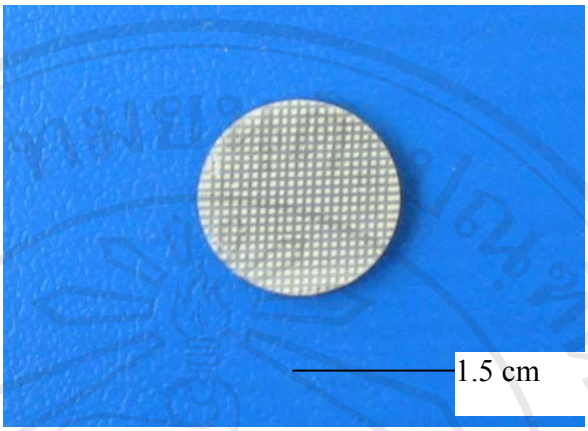

Figure 4.42 Top view photograph of the composite.

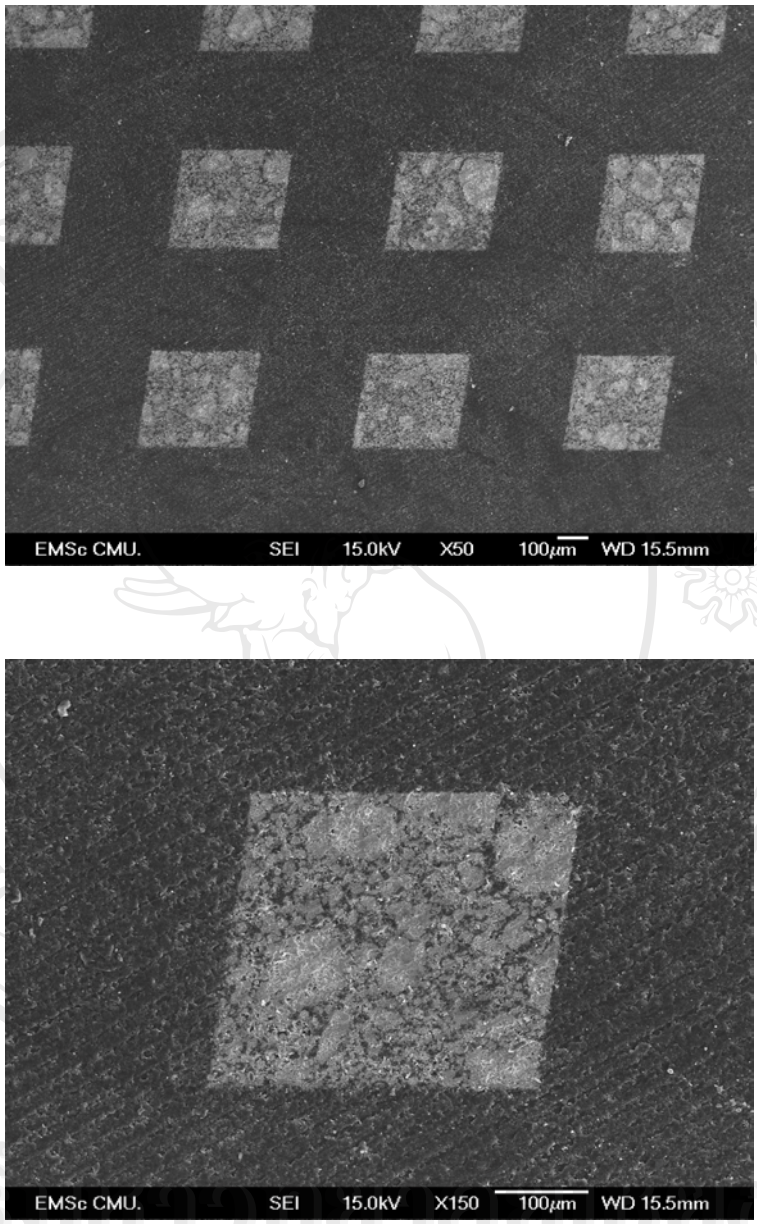

Figure 4.43 The typical SEM micrographs of top view of PZT/epoxy resin composites.

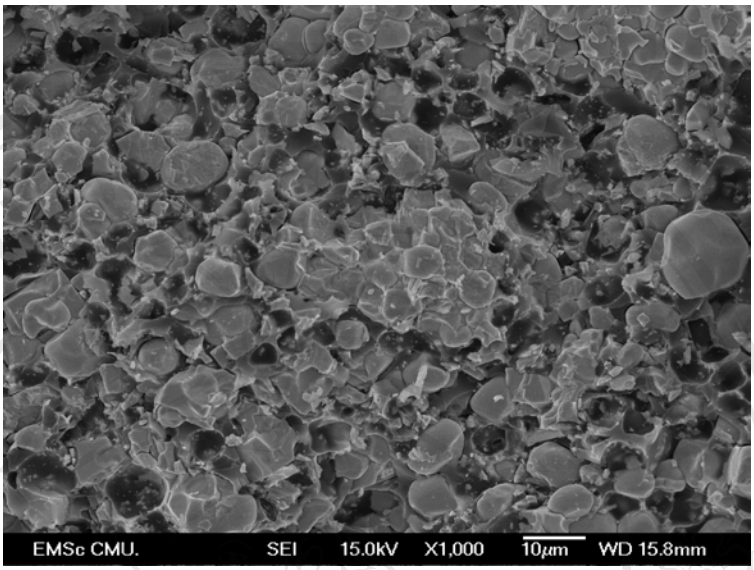

(a)

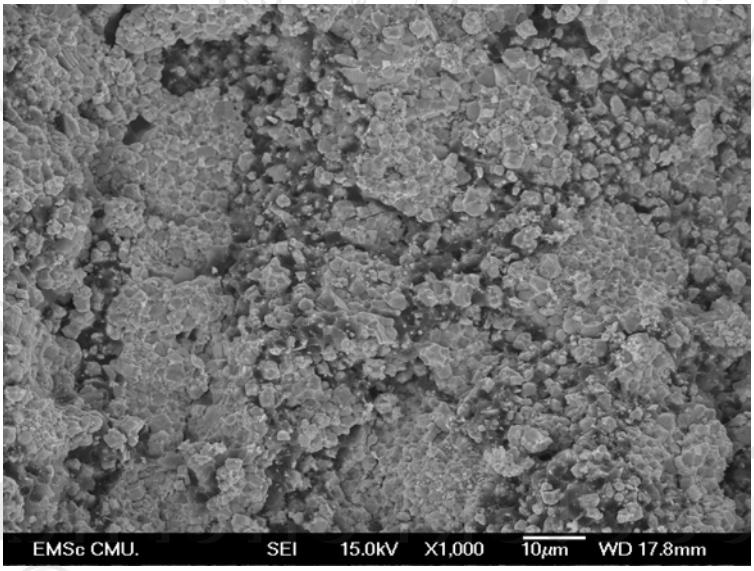

(b)

Figure 4.44 SEM micrographs of PZT/epoxy resin which PZT composites employing powders prepared from mixed oxide route (a) and spray dry techniques (b).

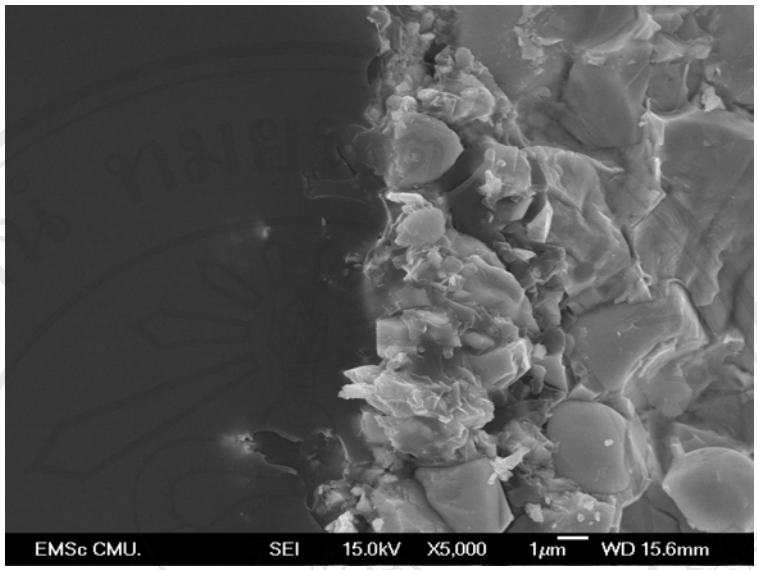

(a)

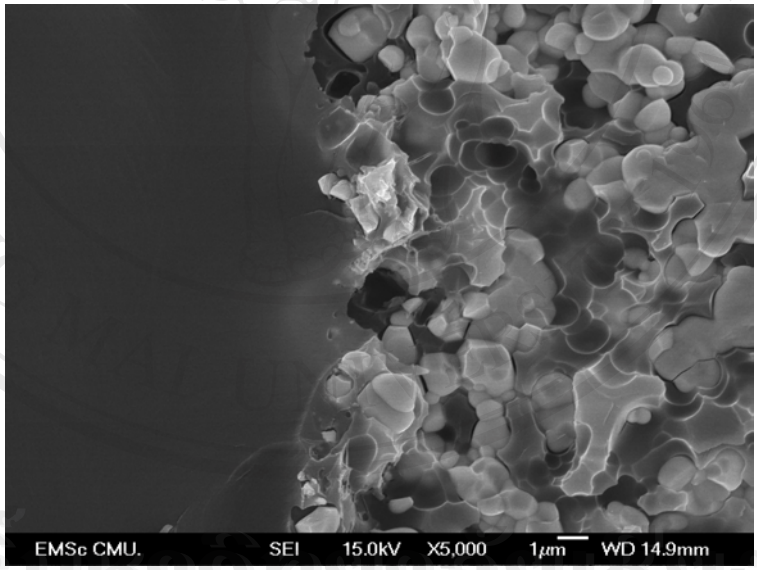

(b)

Figure 4.45 SEM micrographs of cross section of PZT/epoxy resin composites employing powders PZT powder prepared from mixed oxide route (a) and spray dry techniques (b). Dark and brighter areas correspond to the resin and the PZT powders, respectively.

Table 4.2 The relationship of physical properties and sintering temperature of PZT ceramics

Sintering temperature (°C)	mixed oxide PZT			PZT made from spray dried powder			Modified PZT		
	shringkage (%)	porosity (%)	Density (g/cm^3)	shringkage (%)	porosity (%)	Density (g/cm^3)	shringkage (%)	porosity (%)	Density (g/cm^3)
900	-	-	-	20.71	4.49	7.65	13.05	9.86	7.22
1000	-	-	-	21.36	2.37	7.82	14.60	15.48	6.77
1100	-	-	-	21.61	2.62	7.80	14.43	14.73	6.83
1200	1.02	26.09	5.92	22.15	2.08	7.75	14.89	16.85	6.66
1230	5.13	17.48	6.61	21.67	3.87	7.70	15.23	19.10	6.48
1250	5.58	11.86	7.06	21.44	4.37	7.66	15.19	10.99	7.13